Estimation of water requirements in agriculture at a basin scale: THE CASE STUDY OF THE AUDE BASIN

Written by the student:
Filippo Tobia Imbesi Monorchio
302746

Supervised by:
Professor Stefania Tamea
Tutor from the Company: Marta Debolini

Master thesis in Environmental Engineering
Climate Change Track

DIATI
Department of environment, land and infrastructure engineering
Academic year 2024/2025

Abstract

The Mediterranean area, a renowned climate change "hotspot," faces increasing water scarcity that poses a significant threat to its vital agricultural sector. As a contribution to the TALANOA-WATER project, a European-funded PRIMA project, this thesis aims to quantify the future evolution of agricultural water requirements and assess climate-driven impacts on crop yields in the Aude basin, a representative Mediterranean watershed in southern France.

To achieve this, an enhanced R-based agronomic model based on the SIMETAW framework was developed, validated, and applied. The model simulates the daily soil water balance for key regional crops—including wine grapes, cereals, and fruit orchards—across 33 distinct pedoclimatic zones, driven by an ensemble of downscaled climate projections for the RCP 2.6, 4.5, and 8.5 scenarios. Crucially, the framework assesses crop performance across a range of water availability scenarios, from rainfed to fully irrigated conditions, and incorporates regulated deficit irrigation strategies for quality-oriented crops like PGI and PDO wine grapes.

Results indicate a strong divergence in future irrigation demand that is highly dependent on the emissions pathway, with the basin-wide area-weighted requirement projected to increase significantly under the RCP 8.5 scenario throughout the 21st century. The analysis of yield-water production functions reveals that crop resilience to water stress is highly dependent on soil characteristics. For the near-future period (2030-2060), soil type was found to be a more dominant factor in determining yield outcomes than the differences between climate scenarios, with deep, high-capacity soils providing a crucial buffer against drought stress.

These findings highlight the compounded risk of climate change and soil vulnerability in the Aude basin, underscoring the critical need for integrated, adaptive water management strategies. The developed model proves to be a robust tool for supporting policymaking by delivering key agronomic inputs for a broader and integrated hydro-agro-economic modeling framework.

Acknowledgements

I would like to extend my deepest gratitude to Senior Scientist Marta Debolini. In her role as my company tutor, her patience, professional guidance, and scientific support were invaluable to the production of this thesis. She taught me that a researcher must have a true passion for the pursuit of knowledge and for finding tools to make this world a better place. Even during challenging periods, she always believed in me and treated me with the utmost respect.

A sincere thank you goes to Andrea Borgo, from whom I inherited the initial work for this project. He offered invaluable suggestions and help throughout this process. I was privileged to work alongside him and am certain that he will become a highly valued resource in this research field.

I am also very grateful to the entire INRAE team involved in the TALANOA-WATER project. I want to thank Nina Graveline for her understanding regarding my delays and for her relentless dedication and entrepreneurial spirit in managing such a large project. She truly imparted to me the importance of stakeholder communication and of providing results that are useful not only to the scientific community but to all people involved in this field of study.

A special thanks is also due to David Dorchies, from whom I learned R from scratch. His professionalism, organizational skills, and brilliant mind are a source of inspiration for my future career. A big thank you as well to Juliette Le Gallo and Kévin Orlando; working with you has been an immensely valuable experience.

Finally, I wish to thank the CMCC IAFES division in Sassari for giving me the opportunity to work in a motivational environment full of wonderful people.

Contents

Introduction

0.1 Context and Motivation

The Mediterranean Basin is widely recognized as a climate change "hotspot." It is warming about 20% faster than the global average and is expected to see major changes in rainfall patterns [1]. Projections show a potential decrease in annual rainfall from 10% to 30% by 2100 under high-emission scenarios [1]. Some studies suggest even larger reductions in summer rainfall, which is crucial for agriculture, possibly exceeding 40% in certain areas [2]. These climate changes are making water scarcity worse: river flows are expected to decrease by up to 40% in regions like Southern Europe, while extreme events like long droughts and heatwaves will become more frequent and intense [1]. These climate trends are expected to increase pressure on water resources, making droughts more frequent, longer, and more severe.

Agriculture, which in Mediterranean countries uses the most freshwater (globally around 70%, and can be over 85% of total withdrawals in many Mediterranean countries) [3], is at the center of this crisis. Rising temperatures directly affect how crops grow, changes in rainfall patterns and less snowpack reduce soil moisture and water for irrigation. Altered crop cycles may require changes to farming calendars and affect whether certain crops can be grown. As a result, crop production is threatened, and the sustainability of current irrigation practices is in question. This problem is especially serious for the Mediterranean region, known for its high-value "cash crops" like vineyards, olive groves, and fruit orchards, as well as for growing cereals important for regional food security. The future of these farming systems, which are often the foundation of local economies and cultural heritage, is threatened not only by direct climate impacts but also by increasing competition for water from cities, tourism, and the needs of water ecosystems.

Dealing with these complex and connected problems needs advanced tools for analysis and decision support. The use of crop simulation models for understanding agricultural water dynamics and optimizing irrigation management represents the current state of the art [4]. These models can simulate crop growth, estimate water needs, assess the impact of different irrigation strategies, and evaluate how well adaptation measures work under changing climate and socio-economic conditions. By combining water processes with crop science and water management rules, these tools allow us to measure the trade-offs and benefits, supporting the development of sustainable water management plans and effective irrigation policies. The SIMETAW (Simulation of Evapotranspiration of Applied Water) model, for example, is a framework developed to estimate crop water requirements and irrigation demands based on detailed soil, climate, and crop data [5].

The TALANOA-water project is an important response to these pressures. It aims to develop integrated modeling frameworks that link agro-hydrological systems with socio-economic factors. By calculating the trade-offs between water use, crop yields, and economic results under climate change, the project helps policymakers design adaptive strategies for managing water at the basin level. This thesis contributes to TALANOA-water's goals by improving and using an agronomic model, based on the SIMETAW framework, to estimate irrigation demands and crop yields in the Aude Basin (France). This is a Mediterranean region where climate-driven water stress is already changing the success of agriculture and affecting its typical agricultural products.

0.2 Research Objectives

Considering the growing climate risks for Mediterranean agriculture and the urgent need for effective water management strategies, this study addresses three connected research questions:

- How will climate change alter crop water requirements and irrigation demands in the Aude Basin under low, mid, and high-emission scenarios (Representative Concentration Pathways RCPs 2.6, 4.5, and 8.5, respectively)?
- What are the projected impacts of water stress on agricultural yields for key crops that represent the region's farming (e.g., vineyards, cereals, and other important products)?
- How can integrated agro-hydro-economic modeling help develop sustainable water allocation policies in Mediterranean basins that face increasing water scarcity?

To answer these questions, this thesis develops and uses a modified agronomic model based on the SIMETAW framework, improved with an R library for scenario-based analysis. The main objective is to provide a solid agronomic model that can be used for a detailed assessment of water requirements and can be effectively combined into broader hydro-agro-economic models for full policy support.

Chapter 1

Study area and Data Pre-processing

1.1 Study Area Description: The Aude River Basin

The Aude River Basin has a typical Mediterranean climate, with hot, dry summers and mild, relatively rainy winters. Average annual rainfall varies spatially, from less than 600 mm/year near the coast to over 1200-1500 mm/year in the mountainous areas influencing the basin, with a pronounced rainfall deficit during the summer months [6]. Temperatures can go above 35°C in summer, leading to high demand for water from evaporation and plant use. The basin is often affected by droughts, and its water resources are recognized as being under significant pressure, necessitating dedicated management plans to address quantitative deficits and the impacts of climate change [7]. These conditions put a lot of pressure on water resources, which are vital for the region's large-scale farming, city water supplies, and tourism, especially along the coast. Main management problems include repeated water shortages, conflicts between different water users (farming, domestic use, environment), and the need to keep enough water flowing for the environment in the Aude river and its tributaries, especially during times when water levels are low. The study area (Fig.1.1), consisting of the Aude Médiane and Aude Aval sub-basins, covers approximately 3,288 km^2 across 192 communes in the Occitanie region of southern France and serves as a pilot site for the TALANOAWATER project (TALANOAWATER France Report, 2023) [8].

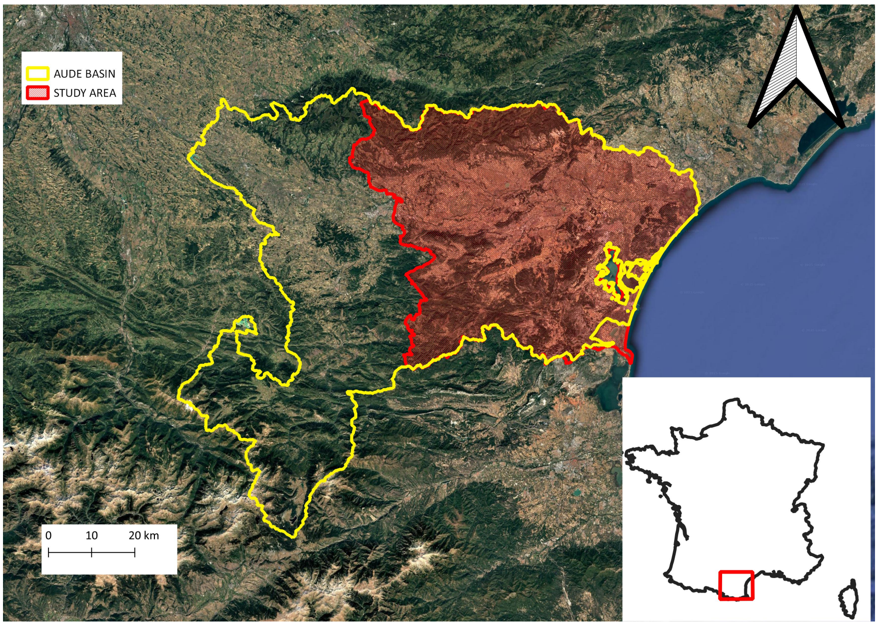

Figure 1.1: Study area of the Aude region

The study area includes two contiguous sub-basins:

- **Aude Médiane (middle section):** Encompasses rolling hills and alluvial plains between Carcassonne and the lower basin, with elevations ranging from 100m to 400m above sea level.
- **Aude Aval (lower section):** Extends from the médiane boundary to the Mediterranean coast, featuring broad floodplains at elevations below 100 m.

The region has about 4,500 farms managing nearly 95,000 ha of cultivated land. About 1,700 of these farms use irrigation systems, covering a total irrigated area of about 23,000 ha. Main land uses include vineyards (a culturally and economically important product), cereal crops, fruit orchards, and pasture. Irrigation water comes from surface water taken from the Aude river and its tributaries, groundwater pumped from alluvial aquifers, and reservoir networks run by collective organizations (ASA - Associations Syndicales Autorisées) and individual users. Whether these water sources can last is a big worry, especially considering future climate projections.

1.2 Data Pre-processing

Before implementing the agronomic simulations, a comprehensive pre-processing of input data was essential to ensure consistency, spatial alignment, and model-readiness. The SIMETAW model requires several environmental inputs including: climate variables, soil properties, and elevation-dependent parameters; prepared at compatible spatial and temporal scales. This section outlines the procedures applied to prepare the datasets used in the modeling workflow, including the harmonization of climatic variables from regional climate models, the classification and aggregation of soil characteristics, and the calculation of reference evapotranspiration. Each step aimed to optimize data accuracy while maintaining computational feasibility, particularly in light of the model's daily resolution and spatial coverage over the Aude Basin.

1.2.1 Climate Data

Accurate simulation of crop water requirements and basin-scale water balances depends on the availability of key climatic variables. These variables are used first to calculate reference evapotranspiration (ET_0) via the Penman–Monteith equation, and second to force the soil water balance model by supplying daily rainfall inputs that recharge soil moisture and determine drainage.

Climatic datasets are obtained from the Drias Climat portal (Météo-France) [9], which delivers daily outputs at an $8km^2$ resolution on the model grid. An ensemble of global and regional climate model projections is included; a synthetic description of the models used appears in Table 1.2. The SAFRAN reanalysis system serves as the reference pseudo-observational dataset for verifying and contextualizing these forcings. The variables present in the models are described in the following table.

Table 1.1: Climatic variables used in the agro-model

Variable	**Description**	**Units**
huss	Near-surface specific humidity	kg/kg
prtot	Total precipitation	mm/d
rlds	Downwelling longwave radiation at the surface	W/m^2
rsds	Downwelling shortwave radiation at the surface	W/m^2
sfcWind	Near-surface wind speed	m/s
tas	Near-surface air temperature	°C
tasmax	Daily maximum near-surface air temperature	°C
tasmin	Daily minimum near-surface air temperature	°C

Table 1.2: GCM–RCM combinations and availability of RCP scenarios (✓= available, ✗= not available)

GCM–RCM	Historical	RCP2.6	RCP4.5	RCP8.5	Period
CNRM–ALADIN63	✓	✓	✓	✓	1951–2100
CNRM–RACMO22E	✓	✓	✓	✓	1950–2100
CNRM–HadREM3-GA7-05	✓	✗	✗	✗	1952–2005
EC-EARTH–HIRHAM5	✓	✗	✗	✓	1951–2100
EC-EARTH–RACMO22E	✓	✓	✓	✓	1950–2100
EC-EARTH–HadREM3-GA7	✓	✓	✗	✓	1952–2099
EC-EARTH–RCA4	✓	✓	✓	✓	1970–2100
IPSL–HIRHAM5	✓	✗	✗	✓	1951–2100
IPSL–WRF381P	✓	✗	✓	✓	1951–2100
IPSL–RCA4	✓	✗	✓	✓	1970–2100
HadGEM2–CCLM	✓	✗	✓	✓	1950–2099
HadGEM2–ALADIN63	✓	✗	✗	✓	1950–2099
HadGEM2–RegCM4-6	✓	✓	✗	✓	1971–2099
HadGEM2–HadREM3-GA7	✓	✓	✗	✓	1952–2099
MPI–CCLM	✓	✗	✓	✓	1950–2100
MPI–RegCM4-6	✓	✓	✗	✓	1970–2100
MPI–REMO2009	✓	✓	✓	✓	1950–2100
NorESM1–HIRHAM5	✓	✗	✓	✓	1951–2100
NorESM1–REMO2015	✓	✓	✓	✓	1950–2100
NorESM1–WRF381P	✓	✗	✗	✓	1951–2100
Safran (Pseudo-Observations)	✓	✗	✗	✗	1958–2024

All the climatic variables listed in Table 1.2 are necessary for the calculations in the following chapters, especially for estimating reference evapotranspiration (ET_0) using the Penman–Monteith formula, which requires relative humidity as an input. Since the climate data provide specific humidity (huss) but not relative humidity, a conversion was required.

Surface pressure was not directly available in the dataset. Instead, a constant pressure value was estimated for each 8 km^2 grid cell based on its mean elevation. Elevation data were obtained from the GTOPO30 global elevation dataset [10], which provides values at a 1 km^2 resolution. For each 8 km^2 model grid cell, the mean elevation was calculated from the underlying GTOPO30 pixels, and the standard barometric formula (Allen et al., 1998) was applied to compute surface pressure. This method assumes that pressure remains constant in time for each cell, which is a reasonable approximation at this spatial scale because daily pressure variations are relatively minor compared to the effect of elevation.

The conversion from specific humidity to relative humidity (hurs) in this study was performed using the "huss2hurs" function from the "convertR" R package (Santander Meteorology Group)[11]. This function follows the methodology described in CMIP5 variable standards and it is widely adopted in meteorology. The process involved calculating first the saturation vapor pressure (e_s) in Pascals considering the mean air temperature(T) in Kelvin with the following formula:

$$\begin{cases} e_s = e_{s0} \exp\left(\dfrac{6808}{T_0} - \dfrac{6808}{T} - 5.09 \log\left(\dfrac{T}{T_0}\right)\right), & \text{if } T \geq T_0 \textbf{ Water} \\ e_s = e_{s0} \exp\left(\dfrac{6293}{T_0} - \dfrac{6293}{T} - 0.555 \log\left(\dfrac{T}{T_0}\right)\right), & \text{if } T < T_0 \textbf{ Ice} \end{cases} \tag{1.1}$$

where: T_0=273.15[K] and es_0=611 [Pa].

Then, the mixing ratio (w) that is defined as the mass of water vapor present in a unit mass of dry air, has been computed directly from specific humidity(q), representing the ratio of the mass of water vapor to the mass of dry air in a given parcel of air. The stauration mixing ratio (w_s) has been calculated using:

$$w_s = \frac{R_d}{R_v} \times \frac{e_s}{p - e_s} \tag{1.2}$$

where: R_d=287.05 $[\frac{j}{kgK}]$ R_v=461.5$[\frac{j}{kgK}]$ are the gas constants for dry air and water vapor and p is the surface pressure $[Pa]$.

Then the relative humidity has been calculated as the ratio of the mixing ratio.

$$\mathrm{RH} = \frac{w}{w_s} \times 100\%. \tag{1.3}$$

In cases where the calculated relative humidity exceeded 100%, values were capped at 100 % to ensure physical consistency.

This procedure ensures that all climatic variables are properly prepared for the Penman–Monteith ET_0 calculation. Only basic quality control steps, such as gap filling and continuity checks, were applied, as the datasets already met the requirements for daily time step and 8 km$^{\mathbf{2}}$ spatial resolution.

1.2.2 Soil Data and Creation of Pedoclimatic Zones

To run the SIMETAW model, two key soil characteristics are required: **soil depth** (SD) and **available water capacity** (AWC). The creation of the final modeling zones, referred to as pedoclimatic zones, was a multi-step GIS-based process designed to produce homogeneous spatial units by integrating soil properties and climatic conditions.

Soil Data Sourcing and Creation of a Unified Soil Map

The foundational soil data for the study area were obtained from the GIS Sol portal, which provides high-resolution maps for metropolitan France. Specifically, soil depth data were sourced from the map of soil depth [12], and available water capacity was sourced from the corresponding map of soil AWC [13].

To make these data suitable for the model, the original categories were converted into representative numerical values.

- The original soil depth categories (less than 30, 30–50, 50–100, and greater than 100 cm) were assigned representative values of 30, 50, 100, and 200 cm, respectively.
- The available water capacity categories (50, 50–100, 100–150, 150–200, and greater than 200 mm per meter) were converted to representative percentage values of 5%, 10%, 15%, and 20% (AWC as mm of water per mm of soil, multiplied by 100).

These two classified data layers were then spatially overlaid using QGIS. This merging process created a single, unified soil map where each polygon represents a unique combination of soil depth and available water capacity class. To avoid excessive fragmentation and to better align the spatial scale with the 8x8 km resolution of the climate data, any resulting polygon smaller than 10 km^2 was dissolved and merged with the largest adjacent neighboring polygon. The resulting spatial distribution of these unified soil classes across the study area is shown in Figure 1.2.

Figure 1.2: Spatial distribution of combined Soil Depth (SD) and Available Water Capacity (AWC) classes after reclassification and merging.

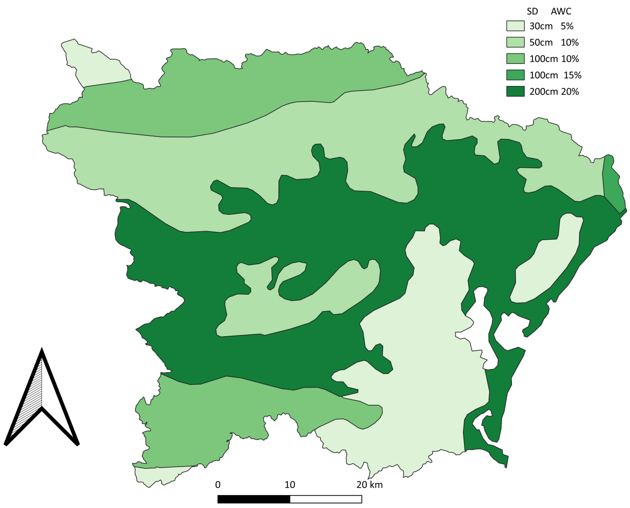

To account for climatic variability across the basin, the study area was subdivided into four broad Climatic Zones. This classification was based on a combination of topographical characteristics and general climatic patterns observed in the climate model data. Within each of these four zones, the climate is considered sufficiently homogeneous for the purposes of applying a single climate forcing time series. The four zones, shown in Figure 1.3, are: **Mountain**: Higher elevation areas, typically cooler and wetter. **Hilly**: Intermediate areas with rolling topography.**Plain**: Lower elevation, flatter inland areas. **Coastal**: The area directly influenced by the Mediterranean Sea, with distinct temperature and humidity characteristics.

Figure 1.3: The four broad Climatic Zones.

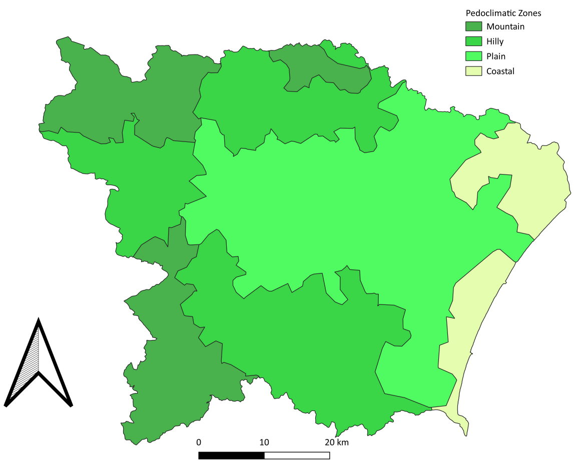

Integration to Create Final Pedoclimatic Zones

The final step was to spatially intersect the unified soil map (Figure 1.2) with the climatic zonation map (Figure 1.3). This final intersection process resulted in the creation of 33 unique **pedoclimatic zones**. Each of these zones is thus defined by a homogeneous combination of climate, soil depth, and available water capacity, forming the fundamental spatial units for all subsequent agronomic simulations.

Figure 1.4 shows the final map of the study area, with each of the 33 pedoclimatic zones labeled. The accompanying legend presents the 15 unique class combinations for these variables. The reason for the difference between the number of zones (33) and the number of legend classes (15) is that the same combination of soil and climate characteristics can appear in multiple, non-contiguous locations within the basin; each distinct area is considered a separate zone for the purposes of modeling. This

Figure 1.4: Pedoclimatic Zones of the Aude study area.

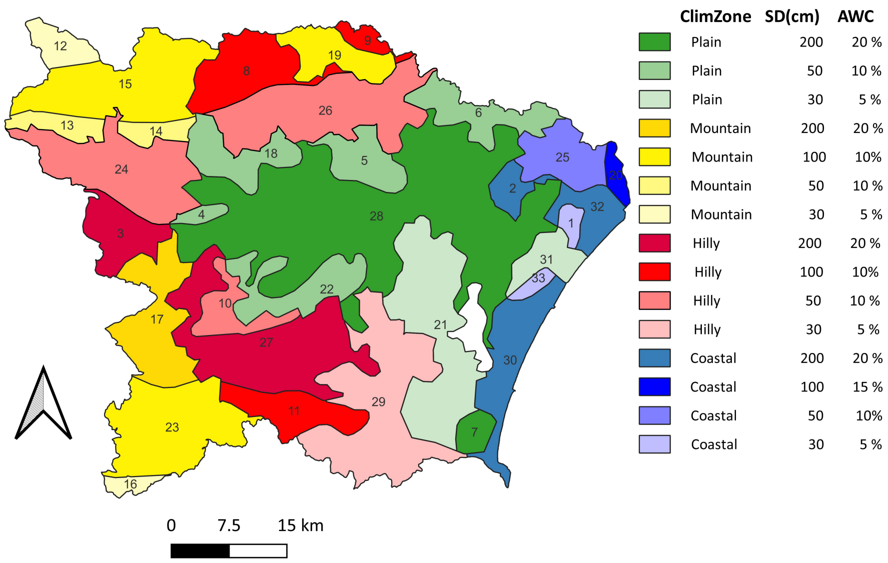

approach allows for both spatial detail and computational manageability, ensuring that each zone used in the agro-model accurately represents its unique pedoclimatic characteristics.

1.2.3 Reference Evapotranspiration

Reference evapotranspiration ($ET0$) is a key component in estimating crop water requirements and assessing the impact of climate change on agricultural water use. In this study, $ET0$ was calculated on a daily basis for the Aude River Basin using two approaches: the standard FAO-56 Penman–Monteith method [14], which uses a fixed surface resistance, and a modified version that accounts for CO_2 fertilization effects by using a variable canopy resistance. Both methods were applied over historical and future climate scenarios using downscaled data from the Drias platform.

The FAO Penman-Monteith equation is the sole standard method recommended by the Food and Agriculture Organization (FAO) for determining reference evapotranspiration from climatic data. This method is physically based and explicitly incorporates both energy (radiation) and aerodynamic (wind and humidity) factors, making it robust across a wide range of climates. The general form of the equation is expressed as:

$$ET0 = \frac{0.408\Delta(R_n - G) + \gamma\frac{900}{T+273}u_2(e_s - e_a)}{\Delta + \gamma\left(1 + \frac{r_s}{r_a}\right)} \tag{1.4}$$

where:

- $ET0$ is the reference evapotranspiration [mm day^{-1}],
- R_n is the net radiation at the crop surface [MJ m^{-2} day^{-1}],
- G is the soil heat flux density [MJ m^{-2} day^{-1}],
- T is the mean daily air temperature at 2 m height [°C],
- u_2 is the wind speed at 2 m height [m s^{-1}],
- e_s is the saturation vapour pressure [kPa],
- e_a is the actual vapour pressure [kPa],
- $(e_s - e_a)$ is the saturation vapour pressure deficit [kPa],

- Δ is the slope of the saturation vapour pressure curve [kPa °C^{-1}],
- γ is the psychrometric constant [kPa °C^{-1}],
- r_s is the bulk surface resistance [s m^{-1}],
- r_a is the aerodynamic resistance [s m^{-1}].

The equation represents the evapotranspiration from a hypothetical reference crop (defined as a well-watered grass surface of uniform height, 0.12 m, and an albedo of 0.23). The numerator contains the two main drivers of evapotranspiration: the energy-driven component (related to net radiation, R_n) and the aerodynamically-driven component (related to wind speed, u_2, and the vapour pressure deficit, $e_s - e_a$). The denominator includes terms that account for temperature and resistances to water vapour transport. For the standard calculation, r_s is fixed at 70 s m^{-1} and r_a is defined as $208/u_2$ s m^{-1}. All necessary parameters were calculated from the daily climate data variables listed in Table 1.1.

Figure 1.5 illustrates the evolution of $ET0$ across the period 1950–2100 using the standard Penman–Monteith formulation. A clear increasing trend is observed throughout the 21st century, particularly under high-emission scenarios such as RCP8.5, where $ET0$ rises significantly—by over 200 mm/year relative to the historical average. This upward trajectory is driven by rising temperatures, reduced relative humidity, and changes in net radiation, all of which amplify the atmospheric evaporative demand. Such results are consistent with expectations under warming Mediterranean conditions, where hotter and drier climates intensify water loss from reference surfaces.

Figure 1.5

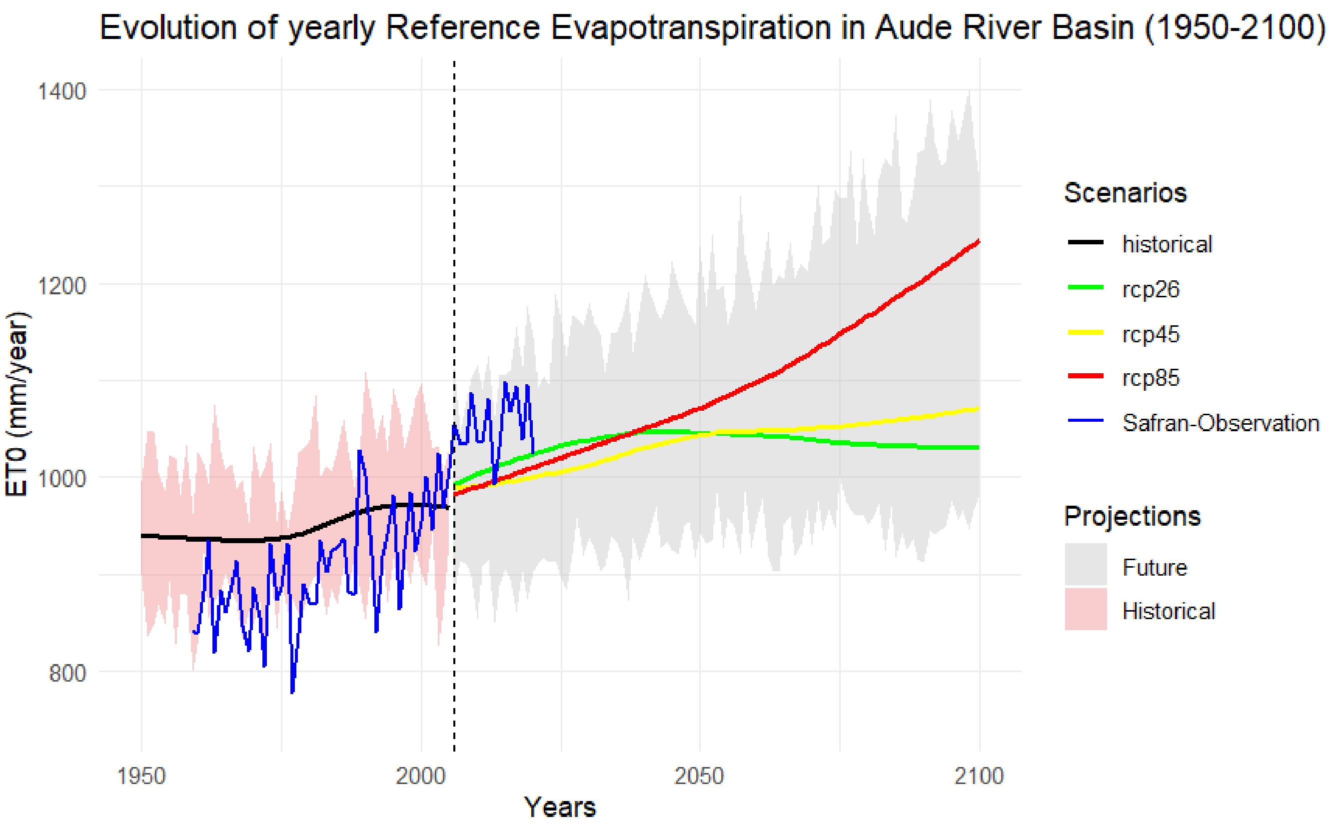

To provide a more nuanced understanding, a second simulation was conducted where the effect of atmospheric CO_2 on plant physiology was incorporated. To account for this CO_2 fertilization effect, the fixed surface resistance (r_s) in Equation 1.4 was substituted with a variable canopy resistance (r_c), which changes based on atmospheric CO_2 concentration. This adjustment models the reduced stomatal conductance of plants under elevated CO_2 levels. The methodology was inspired by previous studies, including Mancosu et al. (2016)[5], where the canopy resistance r_c is expressed as:

$$r_c = \frac{1000}{1.44(14.18 - 0.0112[CO_2])} \quad [s\ m^{-1}] \tag{1.5}$$

Annual average values of CO_2 concentration in *ppm* were sourced from the IIASA RCP Database for each Representative Concentration Pathway (RCP) scenario [15]. These values were applied on a yearly basis: each simulation day within a given year used a fixed CO_2 value representative of that year. The results of this modified simulation, shown in Figure 1.6, contrast sharply with the standard method. Under all scenarios, and most notably under RCP8.5, the increase in $ET0$ is substantially dampened, and in some cases reversed. This highlights the importance of accounting for physiological responses when projecting long-term irrigation demands. However, it is important to note that the empirical formulation used for canopy resistance becomes increasingly uncertain at atmospheric CO_2 concentrations exceeding 550 ppm, a threshold expected to be reached by 2050 under high-emission scenarios. Beyond this point, the assumption of linear or continued stomatal sensitivity to CO_2 may no longer hold, and results should therefore be interpreted with caution.

Figure 1.6

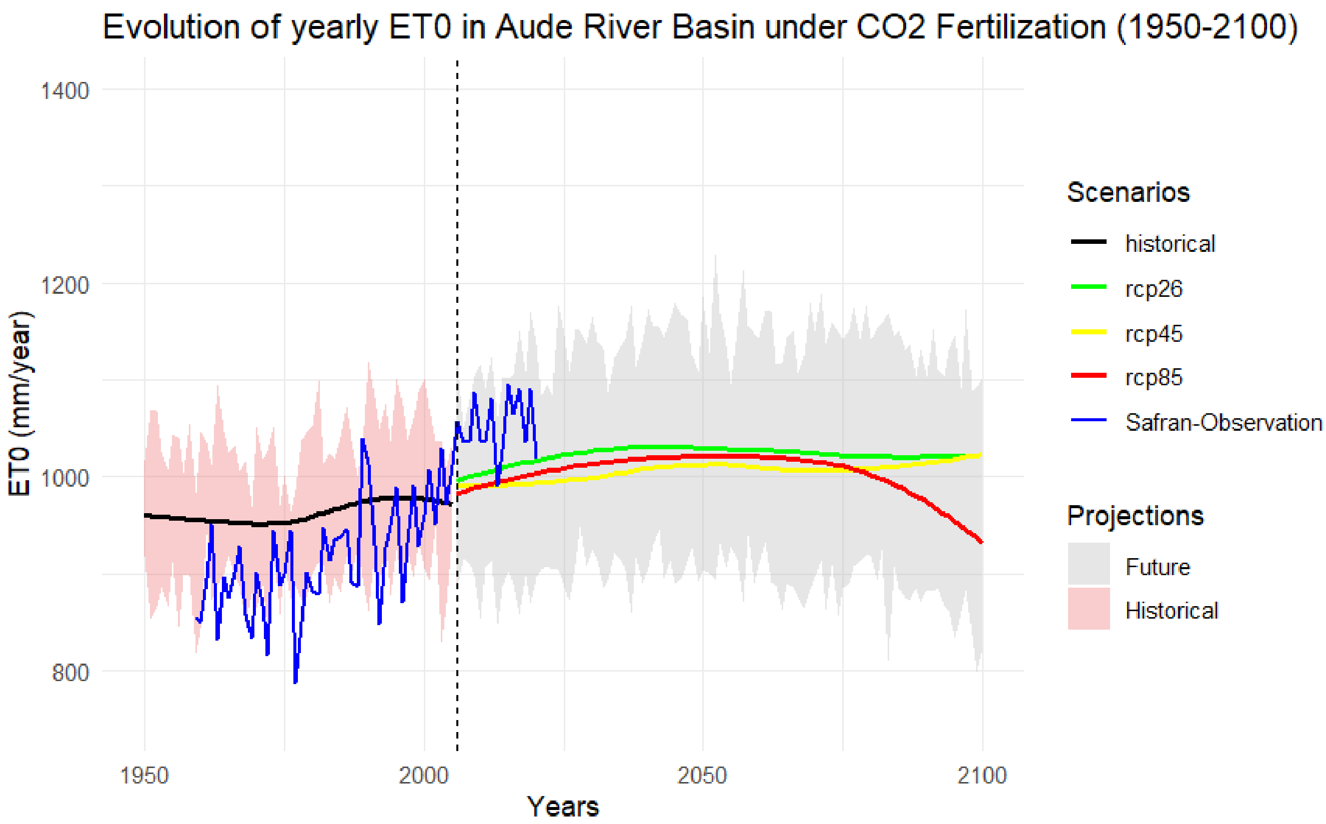

The comparison between the two methods (Figures 1.5 and 1.6) highlights a substantial divergence: while $ET0$ steadily increases under the standard method, the CO_2-adjusted $ET0$ remains largely stable or even declines slightly by mid-century (2050) under elevated scenarios. This result is consistent with findings from FACE (Free-Air CO_2 Enrichment) experiments, which have shown that CO_2 levels near 550 ppm can lead to a 10–15% reduction in evapotranspiration for both C_3 and C_4 crops due to reduced stomatal conductance and altered canopy resistance [16].

For these reasons, the decision was made to use the standard FAO-56 Penman–Monteith equation for all subsequent modeling steps. This method is widely validated, broadly used in both research and practice, and ensures consistency across scenarios without introducing additional uncertainty. While the CO_2 fertilization effect is recognized, its inclusion was limited to exploratory purposes to avoid unnecessary duplication of results. Based on the available literature, it is expected that accounting for CO_2 fertilization could reduce estimated $ET0$ and thus crop water demand—by up to 15-20% by mid-century. This consideration is noted in the interpretation of results, but the core analysis is based on the more conservative and established FAO-56 framework.

These findings provide critical input for the following steps in the agro modeling process, where $ET0$ is combined with soil and crop parameters to estimate irrigation requirements at the pedoclimatic zones level.

Chapter 2

Methodology

2.1 Crop Characteristics

A precise characterization of the crops cultivated within the Aude Basin is fundamental to the agronomic modeling process. The selection of crops for this study was guided by their prevalence, economic significance, and water use patterns within the region, aligning with the objectives of the TALANOA-WATER project [8], which emphasizes stakeholder involvement and the analysis of key agricultural systems in its pilot "living lab" such as the Aude Basin. The chosen crops reflect the diverse agricultural landscape and address common concerns regarding water resource management.

The following crop types are considered in this study:

- **Wine Grapes:** A major agricultural product in the Aude Basin, wine grapes are modeled in several categories:
  - **PGI (Protected Geographical Indication) Vine, PDO (Protected Designation of Origin) Vine, and Non-labelled Vine:** From a biophysical modeling perspective concerning core crop parameters (e.g., growth stage durations, basal crop coefficients), these three types are treated as physiologically identical. The differentiation in their simulation primarily arises from distinct irrigation management strategies and economic considerations, which are applied separately.
  - **Non-labelled Agroecological Vine:** An assessment was made to model this category with a distinct approach reflecting agroecological practices. However, the SIMETAW model, which operates using standardized biophysical parameters, has limitations in explicitly capturing the multifaceted benefits of agroecology (such as improved soil health, biodiversity, or altered nutrient cycling) that are not directly translatable into its input parameter set. It was determined that modifications within SIMETAW for agroecological vines would not yield significantly different water consumption figures directly attributable to the holistic agroecological approach itself, as the model does not account for these complex interactions. Thus, while recognized as a distinct management system, specific agroecological attributes beyond standard irrigation approaches were considered outside the direct parameterization capabilities of the model for this study.
- **Other Perennial Crops:**
  - **Olive:** A traditional Mediterranean crop, significant for its drought resilience and economic value.
  - **Apple:** Representing important fruit orchards in the region that often require irrigation.
  - **Almonds:** Another key orchard crop with specific water requirements, especially during nut development.
- **Annual Crops:**

- **Melon:** A summer cash crop with high water demand during its growing season.
- **Durum Wheat:** A staple cereal crop, cultivated under both rainfed and irrigated conditions.
- **Improved Pasture:** Representing forage production, with water needs varying based on intensity of management and irrigation.
- **Tomato:** A common horticultural crop, often irrigated for optimal yield.
- **Peas:** Selected also as a potential "safety crop." In this study, it is primarily considered under rainfed conditions and evaluated as a possible substitute crop in rotation systems, particularly in scenarios with increased heat or water scarcity where lower-input options might be favored.

The specific input parameters defining the phenological development for each crop are outlined in Table 2.1. This table specifies the key dates that define the various growth stages used in the model: Planting Day (A), the end of the initial stage (B), the end of the crop development stage (C), the end of the mid-season stage (D), and the Harvesting Day (E). These dates are crucial for determining the length of each phenological phase. For perennial crops in this study, Date B is set equal to Date A, signifying a zero-day effective initial stage where mature plants immediately enter the development phase from the start of their seasonal activity (e.g., budbreak).

Table 2.1: Crop Growth Calendar with Phenological Stages

Crop	**Planting Day (A)**	**B**	**C**	**D**	**Harv. Day (E)**
Perennial Crops					
Wine Grapes	**22/March**	22/March	2/May	25/July	**5/Sept**
Olives	**20/February**	20/February	4/May	19/July	**1/October**
Apple	**1/April**	1/April	24/July	19/Sept	**15/Nov**
Almonds	**11/March**	11/March	22/June	13/Sept	**4/October**
Annual Crops					
Melon	**1/April**	18/May	24/July	7/October	**15/Nov**
Wheat	**24/Nov**	31/Dec	16/February	14/April	**31/May**
Improved Pasture	**1/January**	1/April	1/July	30/Sept	**30/Dec**
Tomato	**2/June**	26/June	20/July	18/August	**7/Sept**
Peas	**15/June**	10/July	27/July	20/Sept	**30/Sept**

Following the growth calendar, Table 2.2 provides other key biophysical characteristics and model parameters for each crop. This includes parameters such as the typical maximum rooting depth (mm) and the basal crop coefficients for the initial (Kcb), mid-season (Kcc), and end-season (Kce) stages.

Table 2.2: Crop Characteristics and Parameters

Crop	**Rooth Depth (mm)**	**Kc (A-B)**	**Kc (B-C)**	**Kc (C-D)**	**Kc (D-E)**	**Ky**
Wine Grapes	1500	0.15	0.65	0.65	0.4	0.85
Olives	1450	0.55	0.65	0.65	0.65	1
Apple	1500	0.55	1.2	1.2	0.8	1
Almonds	1220	0.2	0.85	0.85	0.6	1
Melon	1150	0.8	0.95	0.95	0.75	1.1
Wheat	1650	0.15	1.1	1.1	0.15	1.05
Improved Pasture	1000	0.3	0.8	0.8	0.8	1
Tomato	1100	0.15	1.1	1.1	0.6	1.05
Peas	700	0.2	1	1	0.1	1

All these parameters, presented in Table 2.1 and Table 2.2, were established through a review of relevant literature (e.g., FAO Irrigation and Drainage Paper No. 56 [14]), consultation with agricultural research expertise, and specific adaptations to reflect local Mediterranean climatic conditions and typical farming practices prevalent in the Aude Basin. These parameters form the basis for the subsequent calculation of daily crop coefficients.

2.1.1 Spatial Distribution of Cultivated Area

To aggregate the model results to the basin scale and calculate representative averages, data on the spatial distribution of cultivated areas was required. This dataset, providing estimates of the surface area (in hectares) for each crop type within each of the 33 pedoclimatic zones (ZPC), was provided by the TALANOA-WATER project in collaboration with INRAE. The data is based on the **2020 French agricultural census**, which provides information at the municipal level. It should be noted that these data represent the best available estimates but are not exhaustive. For privacy reasons, census data is suppressed for any municipality with fewer than three farms to ensure individual operations cannot be identified. Given the small average size of municipalities in France, this is a frequent occurrence, leading to gaps in the data for certain areas. Therefore, while the dataset provides a robust reflection of the relative distribution and proportion of crops across the basin, the absolute surface area values should be considered representative estimates rather than a complete census.

Figure 2.1 provides an overview of this data by showing the total cultivated area (the sum of all modeled crops) within each zone. This illustrates the concentration of agricultural activity across the study area, with the largest cultivated surfaces located in the central plains.

Figure 2.1: Total cultivated area (sum of all modeled crops) in hectares (ha) for each pedoclimatic zone. Data derived from the 2020 French agricultural census, provided by the TALANOA-WATER project and INRAE.

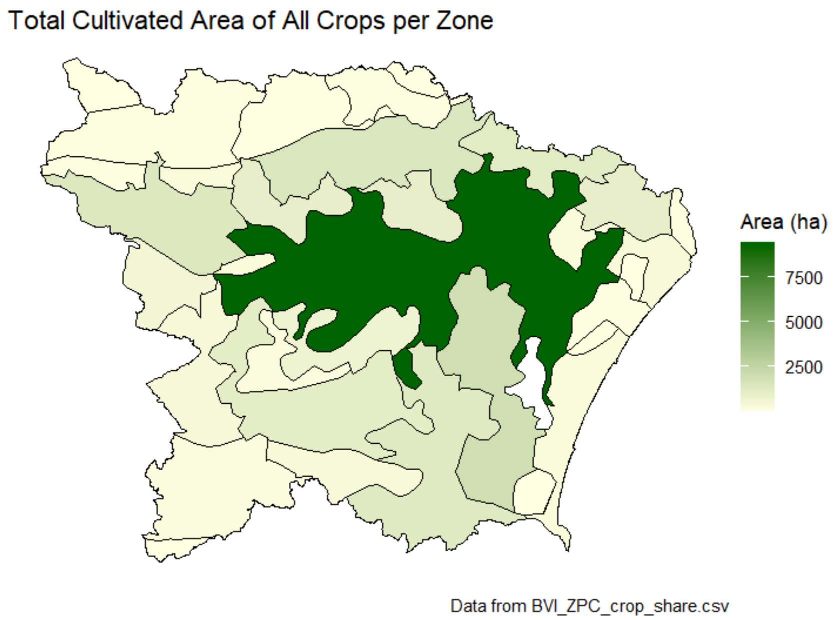

This dataset is critical for the analysis presented in the Results chapter. The area of each crop within each specific zone is used as a weighting factor to calculate basin-wide averages for key metrics, such as Net Application and Applied Water. This ensures that the aggregated results accurately reflect the on-the-ground distribution of agriculture in the Aude basin.

2.2 Methodology for Daily Crop Coefficient Determination

The SIMETAW model computes a daily crop coefficient (Kc_d) which is essential for estimating daily crop evapotranspiration ($ETc_d = Kc_d \times ET0_d$, where $ET0_d$ is the daily reference evapotranspiration). The Kc_d value dynamically integrates the crop's specific water use characteristics across its growth stages and the evaporation from the soil surface. For this study, the ground cover component ($Kc_{\text{Ground\_cover}}$), an optional feature in the model, was not utilized (i.e., effectively set to zero). The daily Kc_d is derived from two main components calculated daily: the crop's basal transpiration coefficient (IKc_d) and the soil surface evaporation coefficient (Ke_d).

The lengths of the four principal phenological phases for each crop, as derived from the dates in Table 2.1, are defined as:

- L_{ini}: Length of the initial stage (days from A to B).
- L_{dev}: Length of the crop development stage (days from B to C).
- L_{mid}: Length of the mid-season stage (days from C to D).
- L_{late}: Length of the late-season stage (days from D to E).

For perennial crops in this study, L_{ini} is effectively zero days as Date B is set equal to Date A (Table 2.1).

The Soil Surface Evaporation Coefficient (Ke_d)

This component, Ke_d, quantifies the evaporation potential from the soil surface, which is particularly influential when the crop canopy is sparse and the soil surface is wet. Its calculation is inspired by dual Kc approaches and methods to estimate evaporation from bare soil [14, 5].

A. Tracking Soil Surface Dryness with Cumulative Dry-Period ET ($ET_{CDP,d}$): The model tracks $ET_{CDP,d}$, defined as the cumulative $ET0$ since the last significant wetting event, serving as an indicator of surface soil moisture status. Let P_d be precipitation on day d, and $ET_{CDP,d-1}$ be this value from the previous day (with $ET_{CDP,0} = 0$).

$$ET_{CDP,d} = \begin{cases} ET0_d & \text{if } P_d \geq 2 \times ET0_d \text{ (significant wetting event)} \\ ET0_d + ET_{CDP,d-1} & \text{if } P_d < 2 \times ET0_d \text{ (drying period)} \end{cases} \tag{2.1}$$

To visualize how this variable operates, Figure 2.2 shows the behavior of $ET_{CDP,d}$ for the year 2016 using Safran observation data. The cumulative ET (green line) steadily increases during dry spells, reaching its largest values during the summer period, when high daily $ET0$ (orange line) and low precipitation create a prolonged accumulation phase. When a significant precipitation event occurs (blue bars), the cumulative ET is reset, starting a new drying period. The large rainfall event in early October 2016 provides a clear example of this reset mechanism, as described by the condition $P_d \geq 2 \times ET0_d$.

Figure 2.2

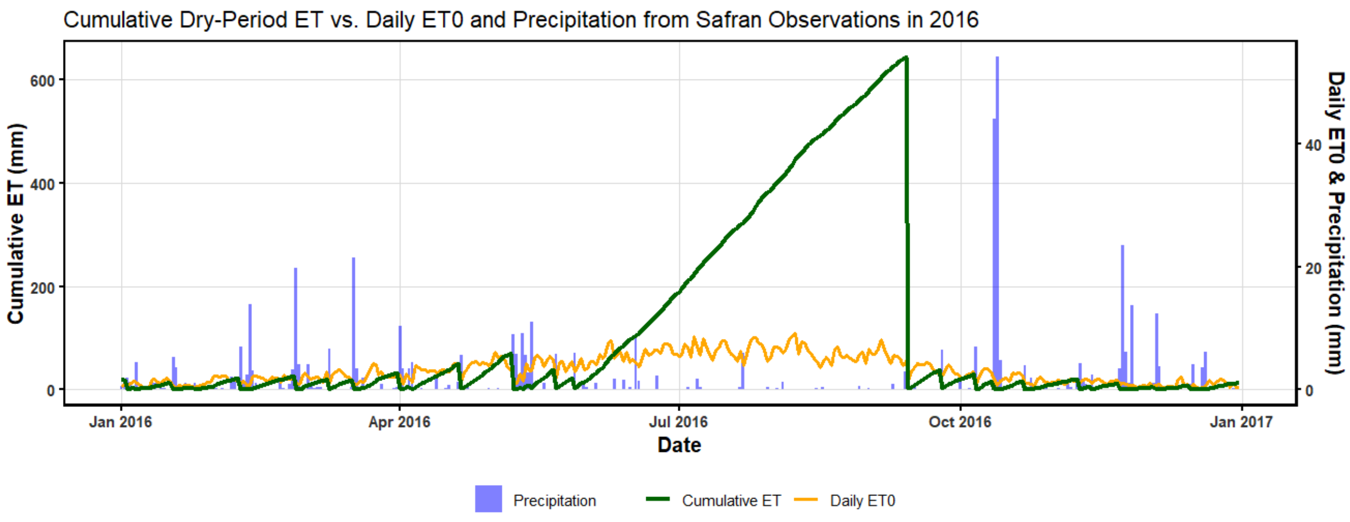

B. Calculating the Daily Soil Evaporation Coefficient (Ke_d): Ke_d is derived from two intermediate factors: one representing the soil-limited evaporation rate ($ke_{factor,d}$) and the other representing an energy-limited upper bound ($Ke_{limit,d}$).

1. The soil-limited evaporation rate factor, $ke_{factor,d}$, represents the declining rate of evaporation from a drying soil surface. It is calculated when $ET_{CDP,d} > 0$ [5]:
$$ke_{factor,d} = \frac{2.54}{\sqrt{ET_{CDP,d}}} \tag{2.2}$$
The constant 2.54 is an empirical coefficient derived from studies on soil evaporation.

2. An upper limit for soil evaporation, $Ke_{limit,d}$, is determined based on daily atmospheric demand:
$$Ke_{limit,d} = 1.22 - (0.04 \times ET0_d) \tag{2.3}$$
The value 1.22 serves as an empirical maximum for this soil evaporation coefficient component when $ET0_d$ is very low, consistent with observed maximum evaporation rates from wet, bare soil surfaces [5].

3. The final daily soil evaporation coefficient, Ke_d, is the minimum of these two factors:
$$Ke_d = \min(ke_{factor,d}, Ke_{limit,d}) \tag{2.4}$$
This formulation ensures that when the soil surface is wet (and $ET_{CDP,d}$ is low, resulting in a high $ke_{factor,d}$), evaporation is limited by the available energy ($Ke_{limit,d}$). As the surface dries (and $ET_{CDP,d}$ increases, resulting in a low $ke_{factor,d}$), the evaporation becomes limited by the soil's ability to supply water ($ke_{factor,d}$).

The Crop's Basal Transpiration Coefficient (IKc_d)

This component, IKc_d, represents the coefficient associated with the crop's transpiration under conditions of no water stress, and it varies daily according to the crop's phenological stage. Its calculation involves several steps:

Foundational Crop-Specific Coefficients: The model begins with three characteristic coefficients for the crop, as specified in Table 2.2:

- Kcb: The basal coefficient for the initial growth stage.
- Kcc: The basal coefficient for the mid-season stage (representing peak water use).
- Kce: The basal coefficient for the end-of-season stage (at harvest or full senescence).

Annual Climate Adjustment of the Mid-Season Coefficient: To reflect the influence of the specific year's climate on peak crop water use, the input mid-season coefficient (Kcc) is adjusted annually.

1. First, the average daily reference evapotranspiration during the crop's mid-season stage for that year ($ET0_{mid,year}$) is calculated. This average is derived from the daily $ET0_d$ values for all days d that fall within the mid-season stage (length L_{mid}, from C to D as per Table 2.1) for the given year:
$$ET0_{mid,year} = \frac{\sum_{d \in \text{mid-season days}} ET0_d}{L_{mid}} \tag{2.5}$$
2. This $ET0_{mid,year}$ is then used to compute the climate-adjusted mid-season coefficient ($Kc_{mid,adj}$) for that year, based on an empirical relationship [5]:
$$Kc_{mid,adj} = Kcc + 0.261 \times (ET0_{mid,year} - 7.3) \times (Kcc - 1) \tag{2.6}$$
This $Kc_{mid,adj}$ serves as the target basal coefficient during the mid-season for that specific year, adapting the generic Kcc to local evaporative demand.

Daily IKc_d Values Across Growth Stages: The IKc_d for any given day d within the growing season (from Date A to Date E) is determined by its growth stage. The construction follows the standard four-stage crop coefficient curve approach [14]. Outside the defined growing season, IKc_d is considered to be zero.

1. **Initial Stage (length L_{ini}, days from A to B):** IKc_d is constant.
$$IKc_d = Kcb \tag{2.7}$$
(For perennial crops, where $L_{ini} = 0$, the crop immediately enters the development stage with $IKc_d = Kcb$ on Day A).
2. **Development Stage (length L_{dev}, days from B to C):** IKc_d increases linearly from Kcb to $Kc_{mid,adj}$. The daily increment, $\Delta Kc_{daily,dev} = \frac{Kc_{mid,adj} - Kcb}{L_{dev}}$, is applied:
$$IKc_d = IKc_{d-1} + \Delta Kc_{daily,dev} \tag{2.8}$$
(where IKc_{d-1} is Kcb on the first day of this development stage).
3. **Mid-Season Stage (length L_{mid}, days from C to D):** IKc_d is constant at the year-specific climate-adjusted value.
$$IKc_d = Kc_{mid,adj} \tag{2.9}$$
4. **Late-Season Stage (length L_{late}, days from D to E):** IKc_d changes linearly (typically decreasing) from $Kc_{mid,adj}$ to Kce. The daily change, $\Delta Kc_{daily,late} = \frac{Kce - Kc_{mid,adj}}{L_{late}}$, is applied:
$$IKc_d = IKc_{d-1} + \Delta Kc_{daily,late} \tag{2.10}$$
(where IKc_{d-1} is $Kc_{mid,adj}$ on the first day of this late-season stage).

Determination of the Final Composite Daily Crop Coefficient (Kc_d)

The final Kc_d for each day is determined by the interaction between the crop's basal transpiration coefficient (IKc_d) and the soil surface evaporation coefficient (Ke_d). The model selects the component that would lead to higher evaporation if the soil surface is wet and exposed, or defaults to the crop's transpiration coefficient if the canopy is more developed, with an overall cap to ensure realistic values:

$$Kc_d = \begin{cases} Ke_d & \text{if } Ke_d > IKc_d \\ \min(IKc_d, 1.22) & \text{if } Ke_d \leq IKc_d \end{cases} \tag{2.11}$$

This logic implies:

- If the potential evaporation from the soil surface (Ke_d) is greater than the crop's basal transpiration coefficient (IKc_d) – typically during early growth stages with sparse canopy and following wetting events – then Kc_d is primarily determined by soil evaporation (Ke_d).
- Otherwise, when the crop's transpiration demand is dominant (e.g., with a more developed canopy), Kc_d is determined by IKc_d. However, IKc_d (and thus Kc_d in this case) is capped at an upper limit of 1.22. This cap represents a plausible maximum for crop coefficients under well-watered conditions, consistent with values reported in literature [14].

This comprehensive daily calculation allows SIMETAW to dynamically adjust the crop coefficient based on crop development stage, annual climatic variations during the mid-season, and daily soil surface moisture conditions, providing a nuanced estimation of crop water requirements throughout the season.

To illustrate the dynamic nature of the daily crop coefficient (Kc_d) calculation within SIMETAW, Figure 2.3 presents a comparison of the final daily Kc_d values for melon, using Safran observational data for two climatically distinct years: 1963 and 2016. These years were selected to demonstrate the model's response to different levels of atmospheric evaporative demand.

Figure 2.3

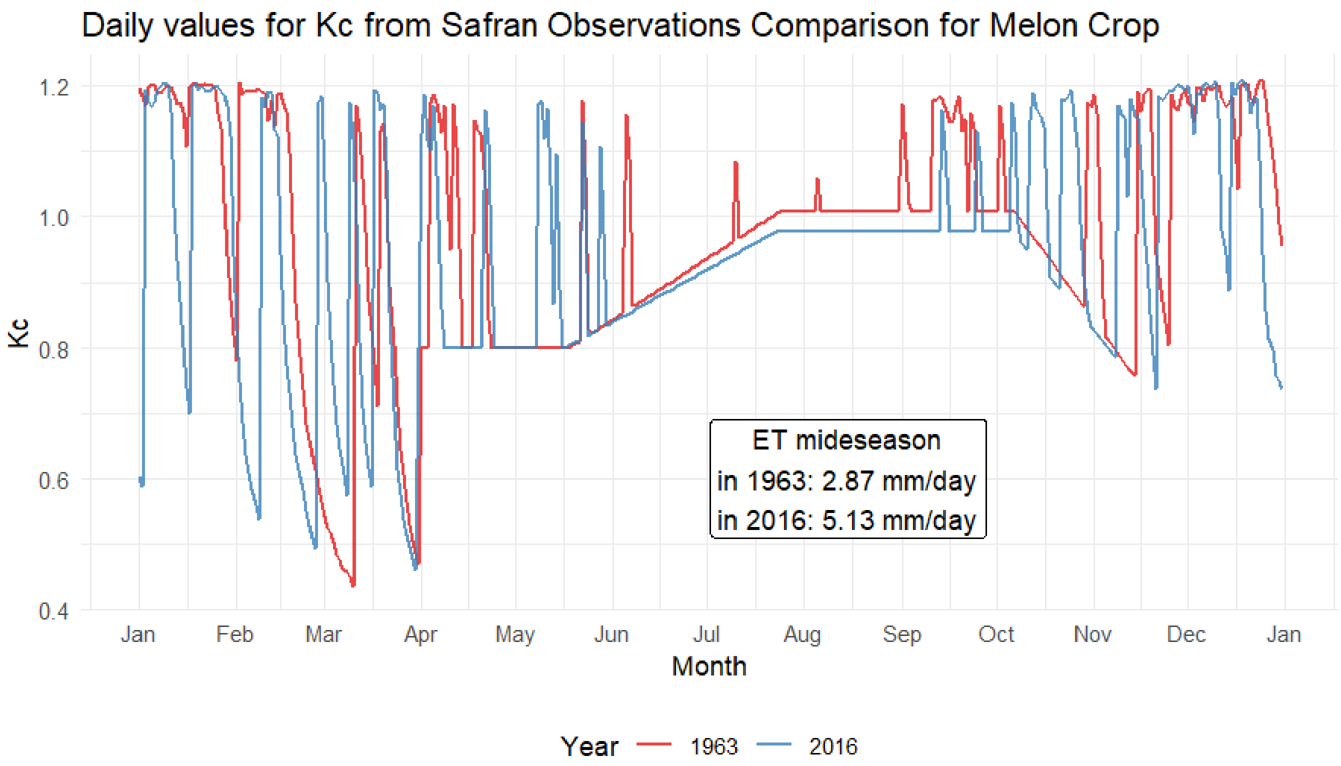

The figure clearly shows the practical application of the climate-adjustment methodology. The most significant difference between the two curves is the height of the mid-season plateau. For the year 2016, which experienced a higher average mid-season reference evapotranspiration ($ET0_{mid,year}$ of 5.13 mm/day), the model calculated a higher adjusted mid-season coefficient ($Kc_{mid,adj}$). This results in the higher blue curve during the peak of the season (approximately August and September). Conversely, for 1963, with a lower $ET0_{mid,year}$ of 2.87 mm/day, the calculated $Kc_{mid,adj}$ and the corresponding mid-season plateau (red curve) are visibly lower. This comparison directly visualizes the effect of the climate adjustment described in the methodology.

Furthermore, the daily fluctuations, particularly during the initial and development stages (April-July), are a result of the daily interplay between the basal crop coefficient (IKc_d) and the soil evaporation coefficient (Ke_d). These variations differ between the two years, reflecting the unique daily sequences of rainfall and ET0 that influence soil surface wetness.

This example highlights how the SIMETAW methodology moves beyond a static, pre-defined crop coefficient curve. It produces a daily Kc_d value that is responsive not only to the crop's phenological development but also to the specific inter-annual and daily variability of the local climate, thereby providing a more nuanced and realistic estimation of crop water requirements.

2.3 Irrigation Methods

An essential component of this study is the characterization of the irrigation methods used in the Aude basin, as the efficiency and operational characteristics of these systems directly influence water demand. This section provides a brief overview of the four irrigation methods considered and details the methodology used within the SIMETAW framework to define the parameters that govern irrigation scheduling.

The following irrigation systems, common in the study region, were modeled:

- **Drip Irrigation:** A high-efficiency micro-irrigation method that delivers water slowly and directly to the crop's root zone through a network of pipes and emitters. This minimizes water loss from evaporation and runoff.
- **Sprinkler Irrigation:** A method that mimics natural rainfall, spraying water over the entire field. It is versatile but can be subject to higher evaporative and wind-drift losses compared to drip systems.
- **Micro-Sprinkler Irrigation:** A hybrid system that uses low-pressure sprinklers to distribute water over a limited area near the crop, offering better water targeting than conventional sprinklers but wider coverage than drip emitters.
- **Gravity Irrigation:** A traditional method where water is distributed across the field by gravity through furrows or by flooding. It is often characterized by lower efficiency due to significant water losses from runoff and deep percolation.

The key operational parameters assumed for each of these systems, which form the basis for the model's calculations, are summarized in Table 2.3.

Table 2.3: Irrigation Parameters

Irrigation Method	**AR** (mm/h)	**DU** (%)	**Time** (h)	**NA** (mm/day)	**Loss** (mm/day)
Drip	0.70	85%	24	14.28	2.52
Sprinkler	3.20	75%	12	28.80	9.60
Micro-Sprinkler	1.30	80%	24	24.96	6.24
Gravity	11.20	64%	8	57.12	32.48

The parameters in Table 2.3 are defined as follows:

- **Application Rate (AR)** [mm/h]: The rate at which water is applied to the field by the irrigation system during its operation.
- **Distribution Uniformity (DU)** [%]: A measure of how evenly water is applied across the field. A higher DU indicates a more efficient and uniform system. For the Gravity method, the effective DU of 64% shown in the table is derived from an assumed potential system uniformity of 75% adjusted for a typical surface runoff loss of 15% (i.e., $0.64 \approx 0.75 \times (1 - 0.15)$). For all other systems, runoff is considered negligible.
- **Time** [h]: The maximum daily operating time for the system.

- **Net Application (NA)** [mm/day]: The calculated net amount of water that effectively infiltrates the root zone in a single day of operation ($NA = AR \times Time \times DU$).
- **Loss** [mm/day]: The amount of water applied but not effectively reaching the root zone due to system inefficiencies ($Loss = (AR \times Time) - NA$).

2.3.1 Irrigation Scenario Setup and Day-Independent Parameters

Before simulating the daily soil water balance, the model calculates a set of key parameters for each crop and year. These parameters define the potential water use, stress thresholds, and the baseline for different irrigation scenarios.

2.3.2 Key Crop Water Use and Stress Threshold Parameters

The following parameters are determined for the entire growing season and are independent of daily irrigation decisions:

Potential Crop Evapotranspiration (ETc_d): This is the potential daily water use of the crop under optimal conditions, calculated as the product of the daily reference evapotranspiration ($ET0_d$) and the daily crop coefficient (Kc_d), as detailed in Section 2.2.

Seasonal Potential Crop Evapotranspiration ($CETc_{MAX}$): This value represents the total potential water requirement of the crop over its entire growing season (from planting, Date A, to harvest, Date E). It is calculated by summing the daily ETc_d values for each day within the growing season. The model also determines the annual maximum ($CETc_{MAX}$) and minimum ($CETc_{MIN}$) values of this seasonal total across the entire simulation period.

Yield Threshold Depletion (YTD_d): The model establishes a daily threshold of soil water depletion which, if exceeded, will cause crop stress and potential yield loss. This threshold is not constant; it varies with the crop's phenological stage to reflect differing sensitivity to water stress.

- During the **initial stage**, the YTD is more restrictive, calculated based on the Allowable Depletion (AD) applied to only the top one-third of the Plant Available Water (PAW). This reflects the crop's shallower, more vulnerable root system.
- During the subsequent **development, mid-season, and late-season stages**, the YTD is calculated based on the AD applied to the full PAW of the effective root zone. This represents the stress threshold for the mature plant.

An off-season YTD is also calculated, based on the water available in the top meter of soil (assuming an AD of 50% applied to 30% of this layer). While irrigation does not occur in the off-season, this parameter is used as a baseline for the soil's water state at the beginning of the growing season in subsequent calculations.

Estimated Irrigation Water Requirement under Full Capacity ($ETaw_c$): The model computes an initial estimate of the seasonal net irrigation water requirement needed to achieve full potential yield, assuming no in-season rainfall. This value ($ETaw_c$) is used to make a first estimate of the number of irrigation events required. It is calculated as the total seasonal water need ($CETc_{MAX}$) minus the amount of stored soil water that the model assumes can be safely depleted from the root zone before stress occurs.

$$ETaw_c = CETc_{MAX} - (YTD_{mid} - YTD_{offseason}/2) \tag{2.12}$$

Here, YTD_{mid} is the yield threshold depletion during the mid-season stage, and the subtraction of half the off-season YTD serves as a proxy for the initial usable soil water deficit at the start of the season.

Estimated Number of Full Irrigation Events (NIc): Using the parameters above, the model estimates the theoretical maximum number of irrigation events for a season under a full capacity scenario:

$$NIc = \frac{ETaw_c}{MADc} \tag{2.13}$$

This provides a baseline for the maximum irrigation frequency against which deficit scenarios can be compared.

2.3.3 Irrigation Restriction Scenarios

In Mediterranean regions like the Aude basin, increasing pressure on water resources, exacerbated by climate change, has already led authorities to impose restrictions on water use for agriculture during drought periods, often formalized through prefectural decrees [17]. To analyze the impact of such conditions, this study employs a scenario-based approach using **Deficit Irrigation (DI)**. DI is a water management strategy where the amount of irrigation water applied is deliberately less than the full crop water requirement. This approach is widely studied and modeled to find strategies that maximize water productivity (yield per unit of water) rather than maximizing yield per unit of land, which is critical in water-scarce environments [18].

To simulate these conditions, a **Water Allocation Percentage (WAP)** factor is defined. This factor represents the percentage of the full irrigation amount that is available. For this study, eleven scenarios were defined to cover a full spectrum of water availability:

- **Full Capacity Irrigation (WAP = 100%):** No restriction is applied, representing the baseline for optimal irrigation.
- **Deficit Irrigation Scenarios (WAP = 90%, 80%, ..., 10%):** A series of nine scenarios with progressively increasing water restrictions.
- **Rainfed (WAP = 0%):** No irrigation is applied, representing the crop's reliance on precipitation alone.

Modeling this range of scenarios is essential for assessing crop resilience and identifying trade-offs between water conservation and agricultural productivity . The WAP factor is applied daily to the Management Allowable Depletion as described in Section, directly constraining the amount of water that can be applied during any given irrigation event in the soil water balance simulation.

Specific Management Strategies for Quality-Oriented Crops

Distinct from the general water availability scenarios defined by WAP, a specific management strategy was implemented for quality-oriented crops like PGI and PDO wine grapes. In viticulture, regulated deficit irrigation is often practiced not just to save water, but to manage vine vigor and improve grape quality (e.g., concentration of sugars and polyphenols). To simulate this practice, a **Soil Water Depletion Percentage (SWDPc)** factor was introduced.

This factor is a daily coefficient (ranging from 0 to 100%) that modifies the calculation of soil water depletion in the model. By setting SWDPc to a value less than 100%, the model calculates the next day's soil water depletion based on a "perceived" depletion that is lower than the actual value ($SWD_{d-1} \times SWDPc/100$). This effectively slows down the rate at which the modeled depletion reaches the irrigation trigger threshold (MAD), forcing irrigation to be applied less frequently and thus reducing the total seasonal water application. This approach simulates a deliberate management choice to maintain a certain level of water stress.

For this study, the following SWDPc strategies were applied:

- For **PGI wine grapes**, where regulations on irrigation are less strict, the SWDPc was set to 70% during the initial and development stages, 50% during the mid-season, and 30% during the late (ripening) season.

- For **PDO wine grapes**, where irrigation is more heavily restricted by production rules, a constant SWDPc of 30% was applied throughout the entire growing season.

This parameter allows the model to simulate the nuanced irrigation practices specific to protected wine grape cultivation without altering the fundamental crop physiological parameters like Kc.

The core of the agronomic model is a daily soil water balance (SWB) which simulates the moisture content within the effective root zone of the crop. This calculation is performed iteratively for each day of the simulation period to track soil water depletion, determine crop water stress, and schedule irrigation events. The model runs parallel simulations for two main scenarios: a full capacity (non-stressed) scenario and a deficit scenario that accounts for water restrictions.

2.4 Soil Water Balance Model

The core of the agronomic model is a daily soil water balance (SWB), which is performed for the crop root zone. This calculation is executed iteratively for each day of the simulation period, tracking changes in soil moisture to determine crop water stress and to schedule irrigation events. To analyze the full spectrum of water availability, the model runs parallel simulations for two primary conditions: a "Full Capacity" scenario, which assumes no water limitations, and a "Deficit" scenario, which accounts for water restrictions as defined by the Water Allocation Percentage (WAP).

The central state variable of the model is the **Soil Water Depletion (SWD_d)**, representing the amount of water [mm] depleted from the root zone relative to its Field Capacity (FC) on a given day d. A value of $SWD_d = 0$ indicates the root zone is at field capacity. The daily simulation loop updates this and other variables based on the following sequence of calculations.

2.4.1 Key Parameters for the Soil Water Balance

Before detailing the daily balance, it is necessary to define several key parameters that govern the soil's water holding capacity and the crop's response to water availability.

Effective Rooting Depth (Z_e): The model first establishes the effective rooting depth for the crop in a specific location. This is determined by the minimum value between the crop's potential maximum rooting depth (an input from Table 2.2) and the actual soil depth of the specific pedoclimatic zone. This ensures that the simulated root zone does not exceed the physical limitations of the soil profile.

$$Z_e = \min(\text{Max Rooting Depth}_{\text{crop}}, \text{Soil Depth}_{\text{zone}}) \tag{2.14}$$

Plant Available Water (PAW): The total amount of water that a plant can potentially extract from the soil is the Plant Available Water. It is calculated for the effective rooting depth based on the soil's Available Water Capacity (θ_{AWC}, in %) and the effective rooting depth (Z_e).

$$PAW = Z_e \times \frac{\theta_{AWC}}{100} \tag{2.15}$$

This PAW value [mm] represents the total volume of water stored in the root zone between Field Capacity (FC) and the Permanent Wilting Point (PWP).

Allowable Depletion (AD): A key assumption in the model for determining the onset of water stress is the **Allowable Depletion (AD)**. This is the fraction of PAW that a crop can extract from the root zone without suffering a significant reduction in evapotranspiration. For this study, a default AD value of 50% is used for all crops. This is a widely accepted value for many field and horticultural crops under non-stressful conditions and is consistent with the approach used in the original SIMETAW model [5].

2.4.2 Daily Simulation Loop

For each day d of the simulation, the model calculates the following variables in order:

1. Water Stress Coefficient (Ks_d): When soil water is limited, crops cannot transpire at their potential rate. The model accounts for this by calculating a daily water stress coefficient (Ks_d). This coefficient, ranging from 1 (no stress) to 0 (maximum stress), is calculated based on the previous day's depletion of available water ('Daw'$_{d-1}$, which is the percentage of PAW that has been depleted) relative to the crop's Allowable Depletion (AD) threshold:

$$Ks_d = \begin{cases} 1 & \text{if } Daw_{d-1} \leq AD \\ 1 - \frac{Daw_{d-1} - AD}{100 - AD} & \text{if } Daw_{d-1} > AD \end{cases} \tag{2.16}$$

This formulation ensures that as soil water depletion exceeds the AD threshold, the stress coefficient decreases linearly.

2. Actual Crop Evapotranspiration ($ET_{a,d}$): The actual crop evapotranspiration for the day is then calculated by applying the stress coefficient to the potential rate (ETc_d):

$$ET_{a,d} = ETc_d \times Ks_d \tag{2.17}$$

3. Cumulative Actual Evapotranspiration ($CETa_d$): The model keeps a running total of the actual evapotranspiration during the growing season. This cumulative value is essential for the final yield estimation.

$$CETa_d = CETa_{d-1} + ET_{a,d} \tag{2.18}$$

4. Effective Precipitation (Re_d): Effective precipitation is the portion of daily rainfall (P_d) that is successfully stored in the root zone and becomes available to the crop. It is calculated as the lesser of the daily rainfall amount and the available storage capacity in the root zone on that day (the sum of the existing depletion from the previous day, SWD_{d-1}, and the water lost to actual evapotranspiration on the current day, $ET_{a,d}$):

$$Re_d = \min(P_d, SWD_{d-1} + ET_{a,d}) \tag{2.19}$$

Rainfall exceeding this amount is considered lost to runoff or deep percolation. This calculation is performed for the entire year, but only considered within the growing season for the SWB.

5. Irrigation Application under Full Capacity (NAc_d): The model first determines if an irrigation event would occur under a full capacity scenario (i.e., no water restrictions). An irrigation is triggered if the soil water depletion, after accounting for crop water use and precipitation, reaches or exceeds the system's daily capacity ($MADc$).

$$\text{If } (SWDc_{d-1} + ETc_d - P_d) \geq MADc, \text{ then } NAc_d = MADc, \text{ else } NAc_d = 0.$$

This establishes the irrigation schedule that would be followed in an ideal, non-restricted environment.

6. Irrigation Application under Deficit (NAa_d): The actual net application of water for the day under a given restriction scenario is then determined. This value, NAa_d, is based on the full capacity application (NAc_d) but is limited by the daily available water defined by the Water Allocation Percentage (WAP) and the corresponding $MADa_d$.

$$\text{If } NAc_d > 0, \text{ then } NAa_d = MADa_d, \text{ else } NAa_d = 0. \tag{2.20}$$

This logic ensures that an irrigation event happens on the same day as in the full capacity scenario, but the amount of water applied is scaled down according to the WAP restriction. This step can also be overridden to simulate a fixed irrigation schedule .

7. Daily Soil Water Depletion Update: Finally, the model updates the soil water depletion for both the deficit ($SWDa_d$) and full capacity ($SWDc_d$) simulations. The general formula subtracts any water gains (effective rain and irrigation) from the sum of the previous day's depletion and the current day's water loss.

$$SWDa_d = SWDa_{d-1} + ET_{a,d} - Re_d - NAa_d \tag{2.21}$$
$$SWDc_d = SWDc_{d-1} \times SWDPc_d + ETc_d - P_d - NAc_d \tag{2.22}$$

The value of SWD is not allowed to go below zero (i.e., the soil cannot hold more water than its field capacity). The SWDPc factor, for simulating quality-oriented strategies in crops like wine grapes, is applied during the calculation of $SWDc_d$, modifying the $SWDc_{d-1}$ term to simulate managed deficit conditions as described in Section 2.3.3.

8. Auxiliary Variables: The model also tracks a daily count of irrigation events and the percentage of available water content ('AWC'), which is calculated as $100 - Daw$, where 'Daw' is the soil water depletion expressed as a percentage of PAW.

By iterating through these steps for each day of the simulation period, the model provides a comprehensive, daily time series of soil moisture dynamics, water stress, and irrigation applications for each crop and scenario.

2.5 Yield Estimation under Water Stress

After the daily soil water balance has been simulated for an entire year, the model performs a final calculation to estimate the crop yield. The methodology is based on the linear yield response function proposed by FAO [19], which relates yield reduction to water consumption deficits. A key enhancement in this model is the way it conceptualizes the root zone in different layers to simulate how water stress develops vertically through the soil profile.

2.5.1 Yield Response to Water Stress

The relationship between water consumption and yield is governed by the crop-specific **Yield Response Factor (K_y)**. This factor determines how severely a crop's yield is affected by a reduction in its water use (transpiration) over the growing season. The fundamental relationship is:

$$\left(1 - \frac{Y_a}{Y_c}\right) = K_y \left(1 - \frac{CETa}{CETc_{MAX}}\right) \tag{2.23}$$

where:

- Y_a is the actual harvested yield.
- Y_c is the maximum potential yield, achieved under optimal, non-stressed conditions.
- $CETa$ is the cumulative actual evapotranspiration over the growing season.
- $CETc_{MAX}$ is the cumulative potential evapotranspiration over the growing season (the reference for 100% yield).
- K_y is the dimensionless yield response factor.

A K_y value greater than 1 indicates that the crop is highly sensitive to water stress, experiencing a proportionally larger yield loss for a given water deficit. The K_y values for each crop are specified as input parameters.

2.5.2 Modeling Yield Response from Layered Soil Water Depletion

To provide a more realistic estimate of yield, the model simulates how water stress impacts the crop by conceptualizing the root zone as four vertical quarters, or layers. This approach acknowledges that the shallowest part of the root zone stores less water and is subject to drying first, while deeper layers provide a more stable water source. This layered approach is conceptually similar to established agro-hydrological models like SWAP [20]. The final field-level yield is calculated as the integrated result of water availability and use across these four conceptual layers.

1. Reference Yield (Full Capacity): The reference for 100% yield (Y_c) is established from the "Full Capacity" simulation (WAP=100%), where irrigation is assumed to be sufficient to prevent water stress. In this scenario, actual evapotranspiration equals the potential evapotranspiration ($CETa = CETc_{MAX}$), and the relative yield is 100%.

2. Infiltrated Water per Quarter (Conceptual): To simulate the effect of non-uniform water application, the model conceptually divides the field into four quarters. First, the total seasonal water delivered by the irrigation system (WA) is calculated by dividing the total Net Application (NA) by the system's Distribution Uniformity (DU). This total applied water (WA) is then conceptually allocated across the four quarters to estimate the Infiltrated Water (IW_q) in each, reflecting that some parts of the field receive more water than others. This approach is adapted from the SIMETAW framework.

$$\text{Superficial 1st quarter:} \quad IW_1 = WA \times DU \tag{2.24}$$

$$\text{2nd quarter:} \quad IW_2 = IW_1 + \frac{1}{3}(IW_4 - IW_1) \tag{2.25}$$

$$\text{3rd quarter:} \quad IW_3 = IW_1 + \frac{2}{3}(IW_4 - IW_1) \tag{2.26}$$

$$\text{Bottom 4th quarter:} \quad IW_4 = WA \times 2 - IW_1 \tag{2.27}$$

3. Actual Evapotranspiration per Layer ($CETa_q$): The model estimates the seasonal actual evapotranspiration ($CETa_q$) that can be supported by each of the four conceptual soil layers.

- The first, shallowest quarter ($q = 1$) is the most susceptible to drying. Its contribution to the total crop ET ($CETa_1$) is determined from the daily SWB simulation, which tracks stress in this most vulnerable layer.
- The subsequent, deeper quarters ($q = 2, 3, 4$) have access to more stored water. The model calculates their contribution to total ET ($CETa_2, CETa_3, CETa_4$) by considering the additional water available at greater depths, but the total ET from all layers cannot exceed the potential maximum ($CETc_{MAX}$).

4. Final Field-Average Yield Calculation: Finally, the relative yield for each conceptual layer, $\left(\frac{Y_a}{Y_c}\right)_q$, is calculated using the yield response function:

$$\left(\frac{Y_a}{Y_c}\right)_q = 1 - K_y\left(1 - \frac{CETa_q}{CETc_{MAX}}\right) \tag{2.28}$$

The resulting value is constrained to be non-negative. The final yield for the entire crop is then computed as the average of the yields supported by the four conceptual layers:

$$\text{Final Yield \%} = \frac{\sum_{q=1}^{4}\left(\frac{Y_a}{Y_c}\right)_q}{4} \times 100 \tag{2.29}$$

This approach provides a nuanced estimate of yield loss by acknowledging that as a soil profile dries, a crop will experience increasing levels of stress, with the shallow root sections being affected first before the deeper, more resilient parts of the root system are impacted.

2.6 Model Performance and Validation

The agronomic model used in this thesis was developed based on the SIMETAW framework but implemented in R to facilitate a large number of scenario-based analyses. A key objective of this development was to improve computational efficiency and flexibility. While the previous version was limited to running on a rectilinear grid, the new model is capable of performing simulations directly on irregular geometries, such as the pedoclimatic zones used in this study, in addition to standard grids.

The new implementation resulted in a substantial improvement in performance, primarily due to the vectorization of the soil water balance (SWB) loop. The old model iterated through each grid cell individually for each day of the simulation, whereas the new model performs calculations on the entire spatial domain at once for each daily time step (e.g., ‘variable[,,day]‘). This architectural change drastically reduces computational overhead. A comparative test, run for the tomato crop under a non-restricted irrigation scenario over a large grid area (wider than the study area), showed that the execution time was reduced from 8.2 minutes with the old model to just 22 seconds with the new R-based version, making it over 20 times faster.

To validate the consistency of the outputs, the results from both models were compared. This validation was performed on a grid to allow for a direct comparison, as the old model was limited to this format. Figure 2.4 shows a time series of the calculated Net Application (NA) for a single, representative grid cell over the historical period. The outputs from the new model (NAnew) and the old model (NAold) are nearly identical, demonstrating temporal consistency.

Figure 2.4: Comparison of historical Net Application (NA) time series between the previous model version (NA_old) and the newly developed version (NA_new) for a single representative grid cell, simulated for the tomato crop.

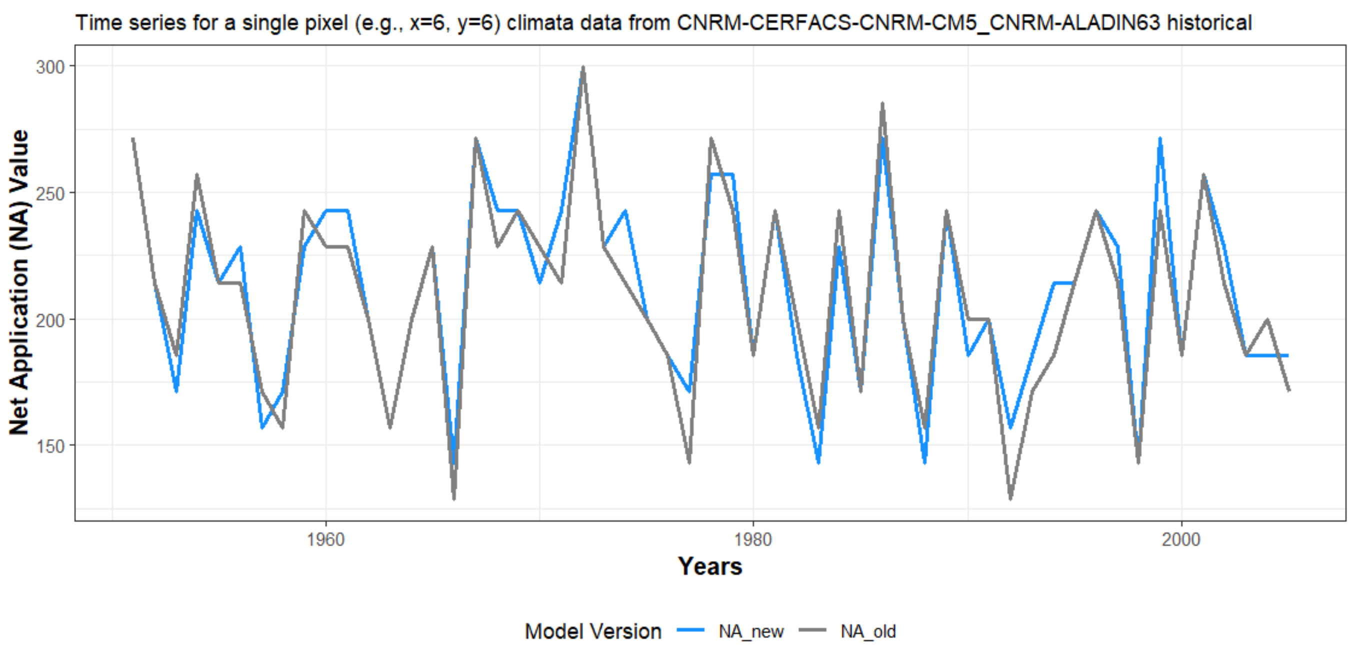

To further validate the model across the entire spatial domain, Figure 2.5 shows the ratio between the Net Application calculated by the old and new models. Across the vast majority of the domain, the ratio is very close to 1.0 (indicated by the bright green color), signifying a near-perfect match. The differences are minimal, with most grid cells showing less than a 2.5% deviation between the two model versions.

Figure 2.5: Spatial comparison of model outputs for the tomato crop, showing the ratio of Net Application from the old model to the new model (NA_old / NA_new) across the model grid. Values close to 1.0 (green) indicate a strong agreement between the two versions.

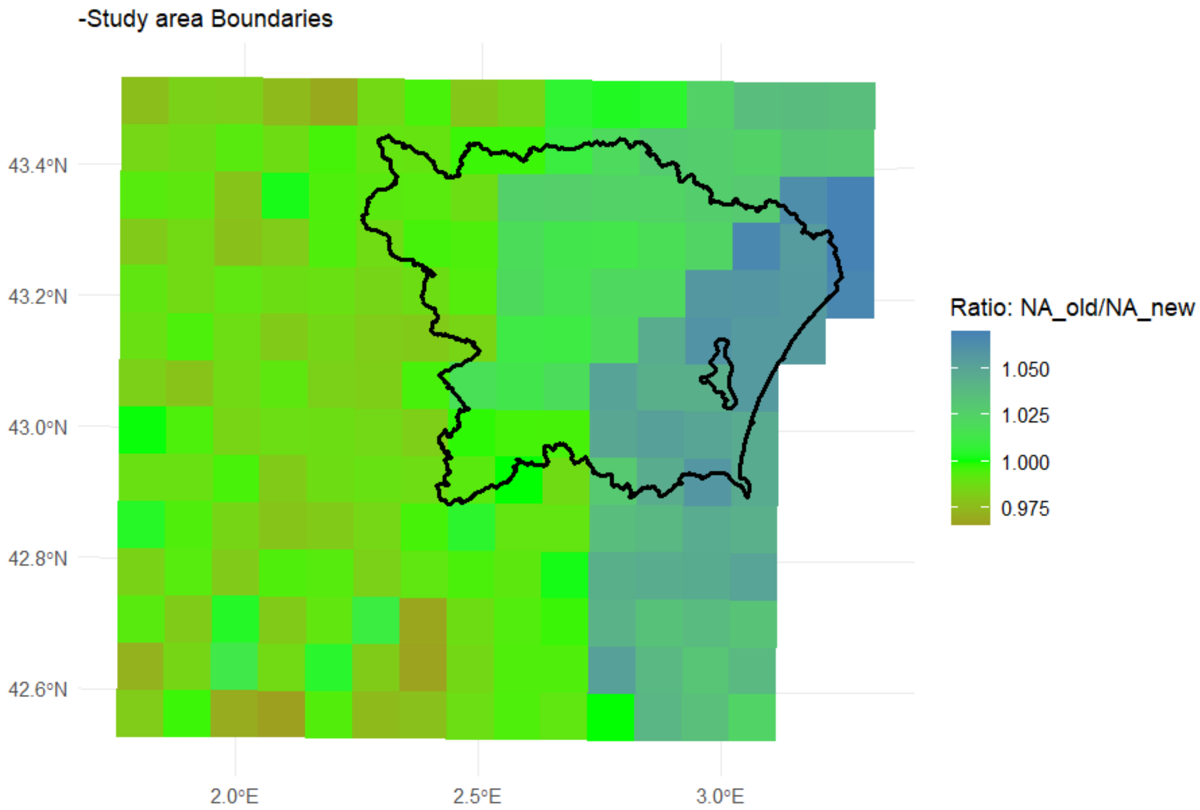

2.6.1 Derivation of Simplified Production Functions for Economic Modeling

A key objective of this thesis is to provide agronomic inputs for a broader, integrated hydro-agro-economic model. The daily soil water balance model produces highly detailed outputs, but for rapid economic scenario analysis, a simplified mathematical relationship between water application and crop yield is required. To achieve this, a continuous production function was fitted to the results for each crop and pedoclimatic zone.

A three-parameter logistic function (also known as a sigmoid curve) was selected to represent this relationship, as it is a standard model for describing crop yield response to inputs in agricultural research [21]. This functional form is ideal as its characteristic "S" shape effectively captures the typical crop response to water: an initial phase with little yield gain, a phase of rapid yield increase with more water, and finally a plateau as the yield approaches its maximum potential.

The equation for the production function is:

$$Y(W) = \frac{a}{1 + e^{-\frac{(W - w_0)}{b}}} \tag{2.30}$$

where:

- $Y(W)$ is the predicted crop yield (as % of maximum) for a given seasonal amount of Applied Water (W).
- a is the maximum potential yield, representing the upper asymptote of the curve.

- w_0 is the inflection point of the curve, corresponding to the water amount at which the yield response is steepest.
- b is a shape parameter that controls the slope of the curve.

The data points for this exercise are the outputs from the detailed soil water balance model, pairing the seasonal Applied Water (W) with the corresponding final relative yield (Y_a) for every year and every water restriction scenario.

To determine the unique parameters (a, w_0, b) for each crop and pedoclimatic zone, a non-linear least squares optimization was performed. This was implemented in R using the 'optim' function with the "L-BFGS-B" method, which minimizes the sum of squared errors between the simulated yield data and the yield predicted by the logistic function. The parameters were constrained to realistic values during optimization (e.g., maximum yield 'a' between 0 and 100).

This process results in a unique, simplified production function for each crop and zone. This function can be straightforwardly integrated into the economic model, allowing for the rapid calculation of yield percentages for any given quantity of applied water, thereby facilitating a wide range of policy and management scenario simulations.

Chapter 3

Results

This chapter presents the primary findings obtained from the application of the agronomic model to the Aude basin. The findings are structured to first ground the model's outputs against observed real-world data and establish a historical baseline of agricultural water use. Subsequently, the chapter details the projected impacts of future climate change on irrigation requirements for key regional crops under the RCP 2.6, 4.5, and 8.5 scenarios. Finally, an analysis of the relationship between water availability and crop yield is presented to assess the region's vulnerability to water stress.

To maintain clarity and conciseness, the results presented will focus primarily on PGI Wine Grapes as a representative perennial crop of high economic importance to the region. Findings for other key crops will be included where necessary to illustrate specific behaviors and provide broader context, thereby avoiding an exhaustive presentation of several hundred graphs for every crop and scenario.

To begin, the model's simulated historical outputs are compared against empirical water use data for the Aude region, provided by the TALANOA-WATER project. These values, shown in Table 3.1, represent typical water doses applied by farmers for various crops in the study area. It is important to note that this empirical data reflects the actual water *applied* in the field, which may come from a mix of irrigation systems with varying efficiencies. The model, by contrast, calculates the *net* water requirement needed at the root zone assuming a standardized, efficient irrigation method. This distinction is important when interpreting the comparison that will follow.

Table 3.1: Empirical irrigation water doses for key crops in the Aude Basin. Data sourced from the TALANOA-WATER project.

Crop	**Empirical Dose (m^3/ha)**
Wine Grapes (PGI)	1500
Wine Grapes (PDO)	600
Wine Grapes (Other)	2000
Olives	2750
Apple	3500
Almonds	2750
Melons	3000
Wheat	1500
Improved Pasture	NA
Tomato	4500

3.1 Future Projections of Net Irrigation Requirements

To provide a basin-scale perspective on future water demand, the results from each pedoclimatic zone were aggregated by calculating the **Area-Weighted Mean Net Application (NA)**. This metric was derived using the crop-specific surface area data described in Section 2.1.1, ensuring that the results reflect the real-world distribution of agriculture across the basin.

Figure 3.1 shows the projected evolution of this basin-wide NA for the three representative crops: Olives, PGI Wine, and Tomato, under a fully irrigated (zero restriction) scenario. The selection of these three crops is intended to represent the diversity of agriculture in the Aude basin. **PGI Wine Grapes** were chosen as they represent a perennial crop of high economic and cultural significance and are subject to specific regulated deficit irrigation strategies that are explored in this study. **Olives** are included as another key perennial, representative of traditional Mediterranean agriculture and known for its notable drought resilience and economic value. Finally, **Tomato** is included as an example of an annual, high-value horticultural crop which typically exhibits high water demand and is often irrigated for optimal yield, providing a contrast to the more drought-resilient perennial crops. It is important to note that NA represents the theoretical net water requirement of the crop at the root zone; the actual gross Applied Water (WA) withdrawn from the irrigation system would be higher after accounting for system efficiencies (i.e., WA = NA / DU).

The results illustrate two critical aspects of future water demand: the long-term trend and the associated uncertainty. The smoothed lines represent the ensemble mean trend for each climate scenario, while the grey shaded area indicates the variability among the individual climate models in the ensemble.

Figure 3.1

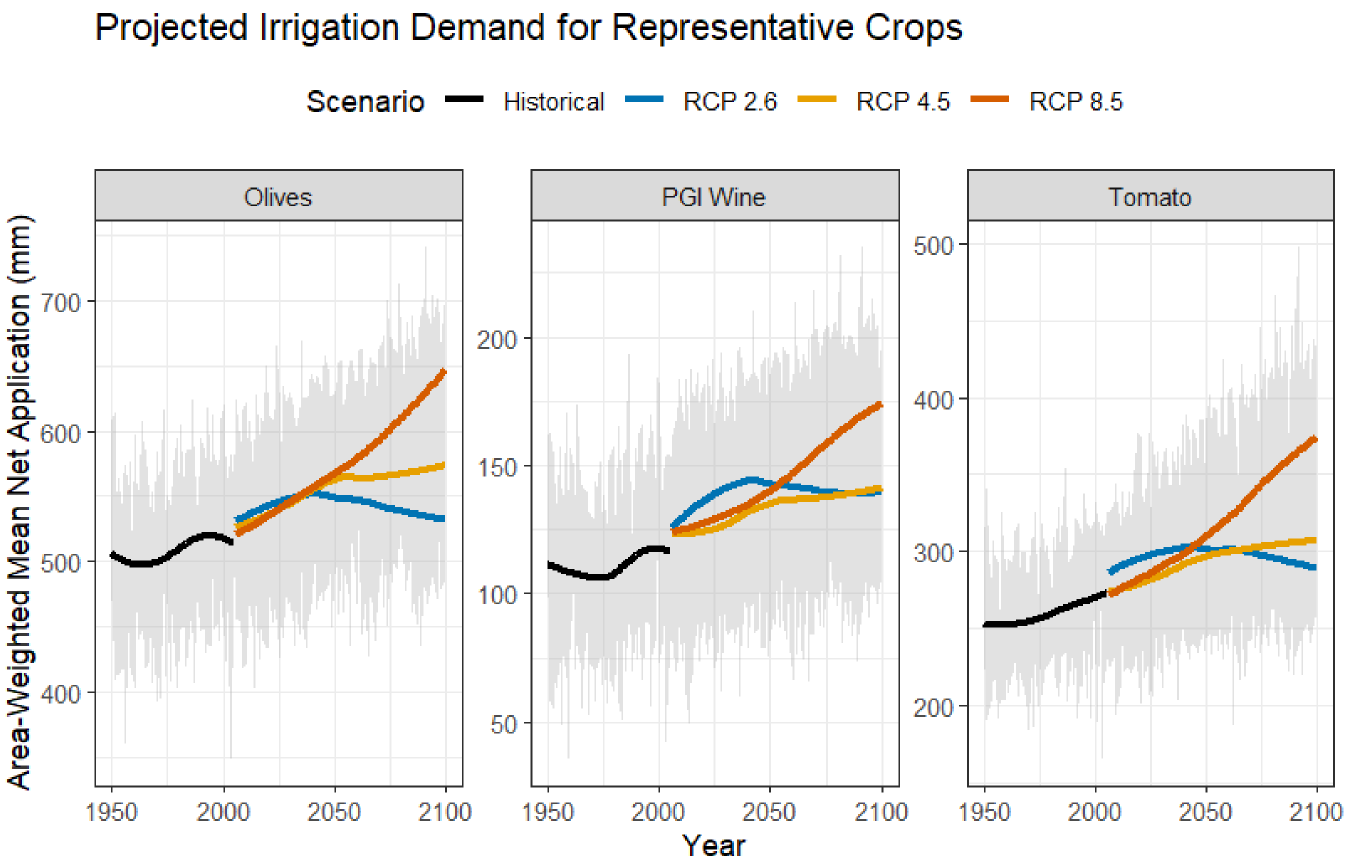

- For all three crops, the **RCP 8.5 scenario** projects a significant and sustained increase in irrigation requirements throughout the 21st century. Relative to current levels, the demand for PGI Wine is projected to increase by approximately **40%** by 2100, while demand for Tomato and Olives is projected to increase by roughly **36%** and **25%**, respectively.

- The **RCP 4.5 scenario** shows a more moderate increase in demand, which tends to stabilize after 2060.

- The **RCP 2.6 scenario** projects a stabilization or even a slight decline in demand by 2100, following a peak mid-century.

3.2 Spatial and Temporal Shifts in Irrigation Demand

To understand how the projected increase in water demand is distributed across the Aude basin, the spatial patterns of Net Application (NA) were compared between the historical period and future scenarios. Figure 3.2 illustrates this comparison for Olives, a key perennial crop, showing the ensemble mean NA for the historical baseline (1985-2005) and for the future period (2040-2060) under the three RCP scenarios.

The historical map (top left) confirms the distinct spatial gradient previously observed, with the highest irrigation requirements concentrated in the warmer, coastal zones (over 550 mm) and lower requirements in the cooler, western inland areas (below 400 mm).

When projected into the future, the magnitude of change is highly dependent on the climate scenario:

- Under **RCP 2.6**, the spatial pattern of irrigation demand remains very similar to the historical period, with only minor increases in NA in some zones.
- The **RCP 4.5** scenario shows a more notable increase in water demand, with the areas requiring over 550 mm expanding further inland.
- The most dramatic change is projected under the **RCP 8.5** scenario. Here, the irrigation demand intensifies across the entire basin. The demand in the central and coastal plains increases substantially, with average requirements exceeding 600 mm across a large portion of the study area—a level of demand not present in the historical baseline.

This analysis demonstrates that unmitigated climate change (RCP 8.5) is projected to not only increase the total volume of water required for agriculture but also to significantly expand the geographical extent of high-demand zones, placing greater stress on the water resources of the entire basin.

Figure 3.2: Spatial comparison of the ensemble mean Net Application (NA) for Olives. The top-left panel shows the historical baseline (1985-2005), while the other panels show the projected demand for the future period (2040-2060) under the RCP 2.6, 4.5, and 8.5 scenarios.

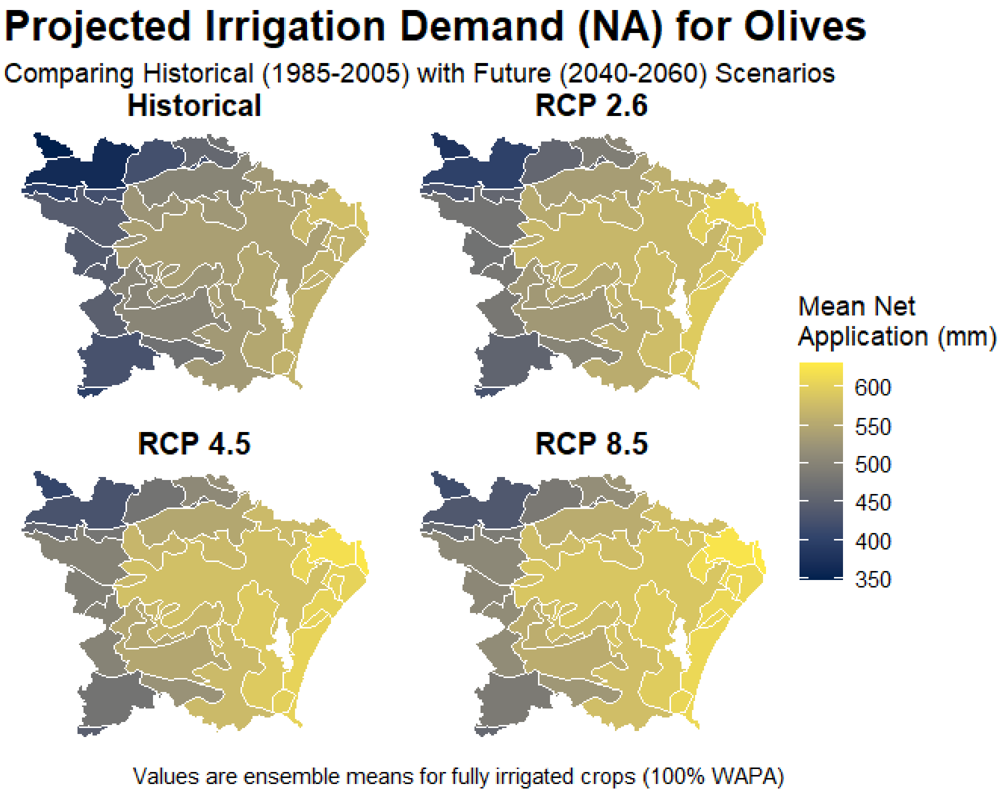

3.3 Impact of Climate Change on Crop Yield

The final stage of the analysis investigates the projected impact of water availability on crop yields, considering both soil characteristics and future climate scenarios. Figure 3.3 presents the yield-water production functions for the period 2030-2060, comparing a shallow, low-capacity soil (Zone 21) against a deep, high-capacity soil (Zone 28).

An initial observation is the effect of the different climate scenarios within this near-future timeframe. Within any single panel, the production function curves for RCP 2.6, RCP 4.5, and RCP 8.5 are clustered closely together. This indicates that for the 2030-2060 period, the projected differences in climate between the scenarios have a relatively minor impact on the overall water productivity of the crops.

In stark contrast, the influence of soil type is dramatic. A comparison between the top row (Shallow Soil) and the bottom row (Deep Soil) reveals a fundamental difference in crop resilience. In the deep soil, yields for all crops are maintained at or near their maximum potential across a much wider range of water application. The shallow soil, however, offers a significantly smaller buffer against water stress, leading to immediate and steep yield declines as water application is reduced. A key result from this analysis is that the model is considerably more sensitive to soil characteristics than to the divergence between climate scenarios in the 2030-2060 timeframe, underscoring that soil health and water holding capacity are primary controls on agricultural resilience.

Figure 3.3: Production functions for the future period (2030-2060). The analysis compares crop yield response to Net Application across two soil types: Zone 21 (Top Row), a shallow soil (300mm depth, 5% AWC), and Zone 28 (Bottom Row), a deep soil (2000mm depth, 20% AWC). The colored lines represent the average trend for three climate scenarios.

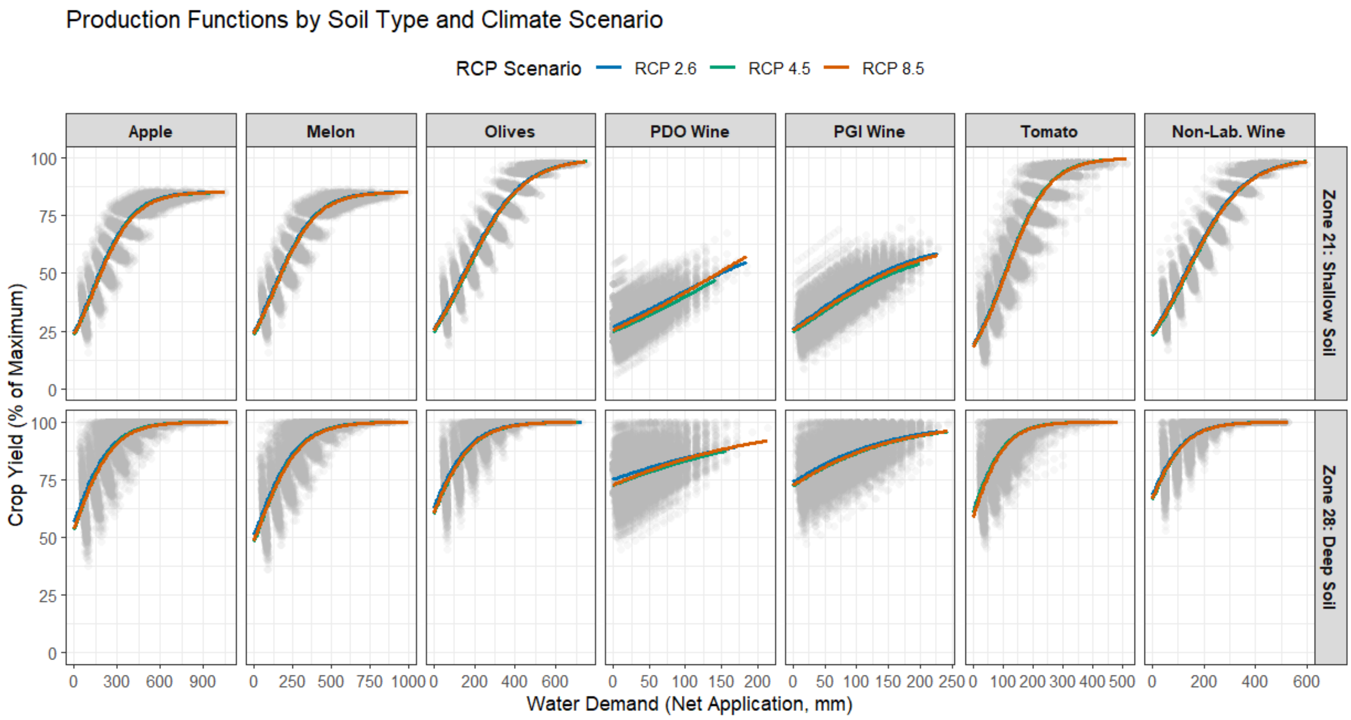

To further investigate the relationship between modeled outcomes and real-world practices, the empirical water doses (from Table 3.1) were compared against the production functions. It is critical to note that the empirical values represent gross *Applied Water*, while the model's production functions use *Net Application*. Therefore, the empirical doses were first converted to an equivalent Net Application by multiplying them by the Distribution Uniformity (DU) of the assumed irrigation method for each crop.

Figure 3.4 shows this comparison for the three representative crops in the resilient, deep soil zone (Zone 28) under the RCP 4.5 scenario. The analysis reveals how the model can help interpret different real-world irrigation strategies:

Figure 3.4: The dashed line indicates the Net Application equivalent of the empirical dose and the corresponding predicted yield.

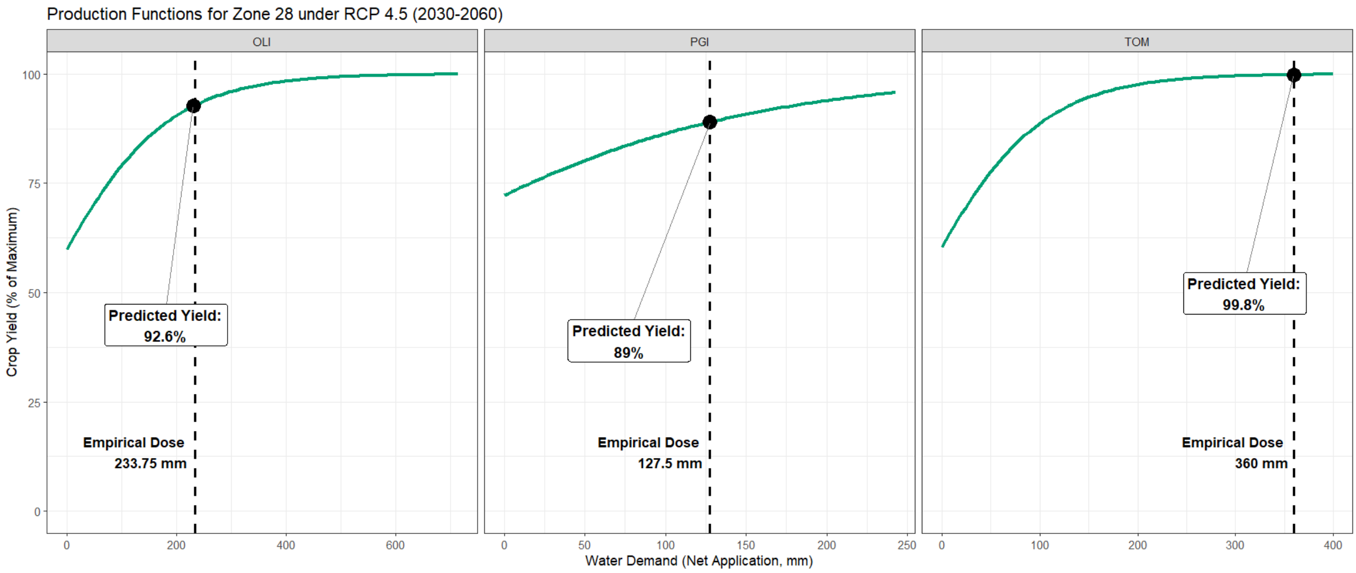

- **For Tomato**, a high-value and water-sensitive crop, the empirical net dose of **360 mm** aligns almost perfectly with the point of maximum yield, predicting a yield of **99.6%**. This suggests that for this crop, standard practice is to irrigate fully to maximize output, as every unit of water provides a significant return.

- **For Olives**, a drought-resilient perennial, the empirical net dose of **233.75 mm** falls on the "shoulder" of the production curve, achieving a high yield of **92.6%**. This reflects a rational economic choice: a farmer may decide that applying significant additional water for a minimal gain in yield is not cost-effective.

- **For PGI Wine**, the empirical net dose of **127.5 mm** corresponds to a predicted yield of just **89%**. This is clear evidence of a managed deficit irrigation strategy, where yield maximization is deliberately sacrificed, likely to enhance grape quality, a common practice for protected designation wines.

This comparison demonstrates the model's utility not just for prediction, but for interpreting the logic behind different, rational farming practices in a water-limited environment.

3.4 Analysis of Specific Management Strategies for Wine Grapes

Beyond analyzing broad climate scenarios, the modeling framework was also used to evaluate the impact of specific, quality-oriented irrigation strategies applied to PGI and PDO wine grapes. As described in the methodology (Section 2.1.3), the Soil Water Depletion Percentage (SWDPc) factor was implemented to simulate regulated deficit irrigation, where water stress is deliberately induced to improve grape quality.

Figure 3.5 illustrates the effectiveness of this approach by comparing the daily irrigation schedule for Non-Labelled (standard), PGI, and PDO wine grapes for a representative year (2015) in Zone 28. The simulation assumes a non-restricted water supply (100% WAP), where each irrigation event delivers 14.28 mm of water. Under the standard approach for **Non-Labelled Wine**, where the goal is to consistently minimize water stress, the model triggered a total of **34 irrigation events** throughout the growing season.

In stark contrast, the managed strategies for quality-oriented grapes show a dramatic reduction in irrigation frequency. The application of the 'SWDPc' factor forces the model to tolerate higher levels of soil water depletion before triggering an irrigation event. For **PGI Wine**, this resulted in only

11 events, a reduction of nearly 70% compared to the standard approach. The highly restrictive strategy for **PDO Wine** was even more pronounced, triggering just **3 events**—a reduction of over 90%.

This analysis demonstrates that the SWDPc parameter is an effective tool for simulating the real-world consequences of regulated deficit irrigation rules. It successfully translates a management choice for inducing water stress into a quantifiable and significant reduction in the number of irrigation events and, consequently, the total volume of applied water.

Figure 3.5: Comparison of the daily irrigation schedules for three wine grape management strategies in 2015 for Zone 28. Each blue marker represents a single irrigation event of 14.28 mm. The total number of events for each strategy is noted on the right.

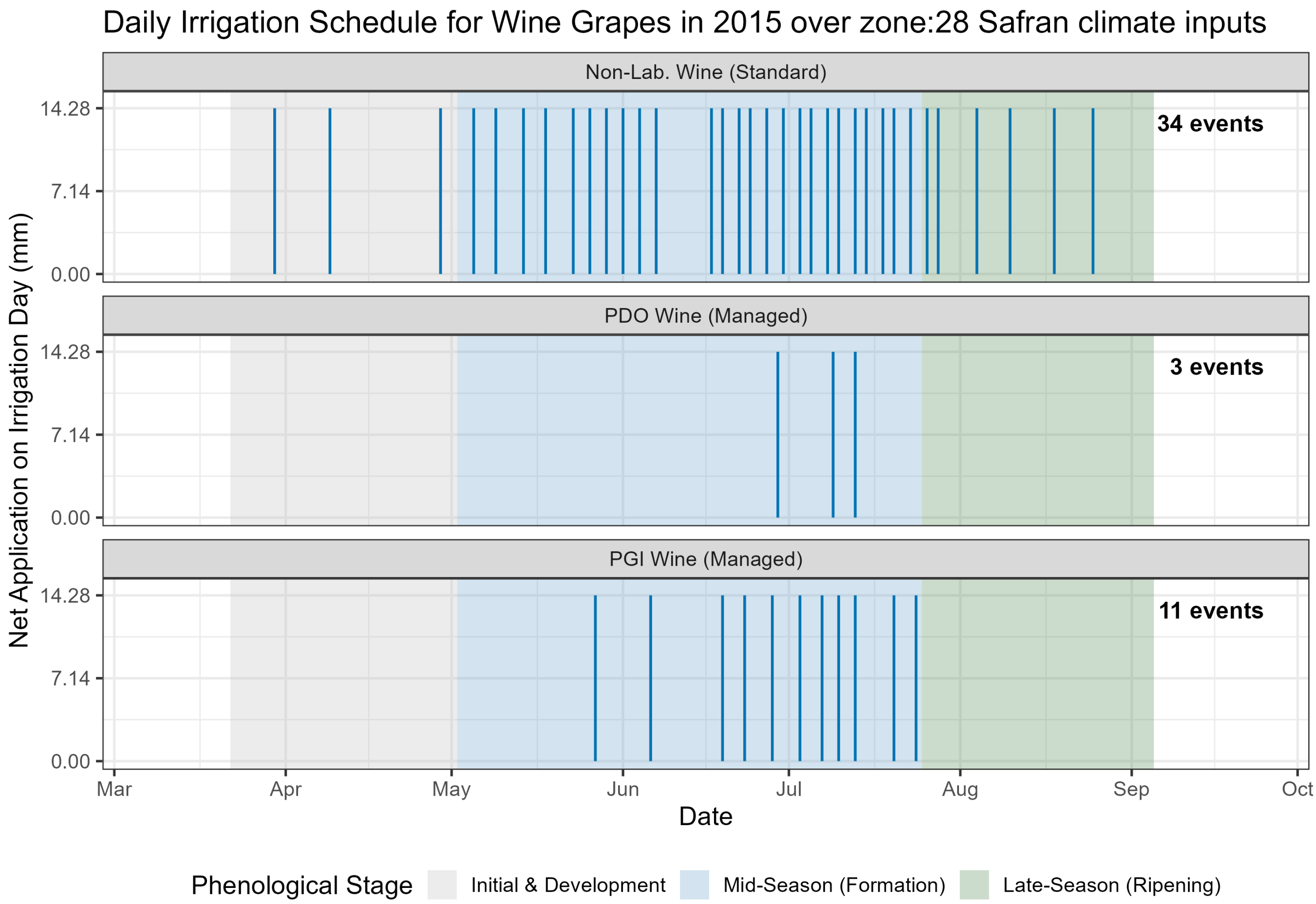

3.5 Assessing Adaptation Strategies: Peas as a Rainfed "Safety Crop"

In addition to analyzing existing agricultural systems, the modeling framework was used to assess the viability of a potential adaptation strategy: the cultivation of peas as a rainfed "safety crop" during the summer. This crop was chosen for its short cycle, but planting it in the Aude basin's most water-stressed period (growing season from June 15 to September 30) represents a significant challenge due to high temperatures and low rainfall.

Figure 3.6 shows the projected mean yield percentage for rainfed peas, comparing the historical baseline (1985-2005) with the future period (2040-2060) across the three RCP scenarios.

The historical results indicate that even under past climate conditions, rainfed summer cultivation is challenging. Average yields ranged from over 60% of the maximum potential in the most favorable zones to below 40% in others. This establishes that achieving high yields without irrigation in summer is difficult.

Looking toward the future, all climate scenarios project a decline in the potential yield for rainfed peas. The effect is most severe under the **RCP 8.5 scenario**, where yields in many central and coastal zones are projected to drop below 30%. The areas capable of achieving yields above 50% shrink considerably, indicating a significant increase in water stress during the summer months.

Figure 3.6: Projected average yield percentage for rainfed Peas. The analysis compares the historical baseline (1985-2005) with the future period (2040-2060) for the RCP 2.6, 4.5, and 8.5 scenarios.

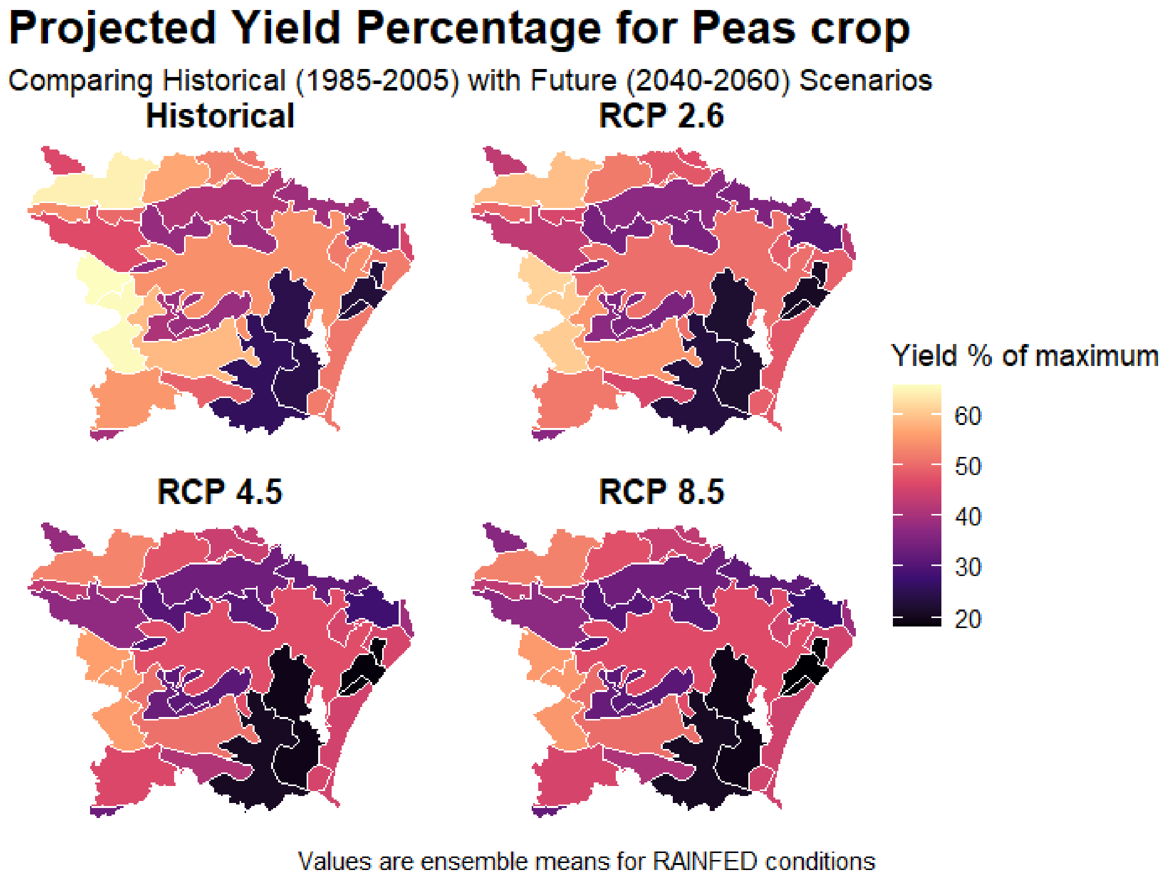

While these are low yields compared to an irrigated crop, they are not negligible. Considering the crop is grown without any irrigation during the driest part of the year, achieving an average yield of $40 - 50\%$ in some areas, even in a future climate, suggests that drought-tolerant summer crops could still play a role as a low-input, risk-mitigation option for farmers. However, the strong negative trend under RCP 8.5 demonstrates that the viability of even this "safety crop" strategy is severely threatened by unmitigated climate change.

3.6 Water Demand for Wine Grapes During Extreme Climate Years

To conclude the analysis, a focused investigation was conducted on the impact of extreme climate years specifically on wine grape cultivation in the most productive area of the basin. The analysis was centered on Zone 28, the most heavily cultivated pedoclimatic zone. To create a more crop-relevant indicator of climate extremes, the Precipitation-to-Evapotranspiration (P/ET0) ratio was calculated using data only from within the wine grape growing season (March 22 to September 5). For the historical period (1976-2005) and each future scenario (2030-2060), the years with the minimum ("Most Arid") and maximum ("Most Humid") growing-season P/ET0 ratio were identified.

The key water balance components for these extreme years are summarized in Table 3.2. The results provide several critical insights into the future vulnerability of viticulture in the region.

Table 3.2: Summary of Water Balance Components for Wine Grapes during Extreme Years.

		Historical		RCP 2.6		RCP 4.5		RCP 8.5	
Variable	**Crop**	**Most Arid**	**Most Humid**	**Most Arid**	**Most Humid**	**Most Arid**	**Most Humid**	**Most Arid**	**Most Humid**
NA (mm)	PDO	51.8	43.1	70.9	66.6	74.0	58.7	73.0	61.1
	PGI	117.0	104.0	135.0	128.0	140.0	122.0	141.0	118.0
	WGI	434.0	404.0	443.0	411.0	464.0	414.0	475.0	409.0
ETa (mm)	PDO	312.0	326.0	340.0	371.0	338.0	349.0	317.0	355.0
	PGI	371.0	381.0	399.0	424.0	399.0	406.0	380.0	407.0
	WGI	558.0	546.0	579.0	563.0	583.0	558.0	588.0	564.0
P/ET0 Ratio (Indicator)		0.261	0.426	0.257	0.430	0.225	0.396	0.222	0.390

First, the analysis of the aridity indicator itself reveals that future droughts are projected to be more intense. The P/ET0 ratio for the "Most Arid" year consistently decreases in the future, from 0.261 in the historical period to as low as 0.222 under the RCP 8.5 scenario. This indicates that the meteorological conditions during the most challenging growing seasons will become even drier.

Consequently, the irrigation required to avoid stress during these future droughts is projected to increase significantly. For PGI wine grapes, the Net Application (NA) in the historical "Most Arid" year was **117.0 mm**. In the future "Most Arid" year under the RCP 8.5 scenario, this requirement rises to **141.0 mm**, an increase of over 20%. This shows that even to maintain the same crop, more water will be needed to get through a future drought than a past one.

Finally, the Actual Evapotranspiration (ETa) provides insight into the level of crop stress. For PDO grapes in the historical period, ETa was lower in the arid year (312.0 mm) than the humid year (326.0 mm), despite higher irrigation. This suggests that even with irrigation, the extreme atmospheric demand during arid years can limit the plant's ability to transpire, indicating a higher level of stress.

This focused analysis underscores a key challenge: future growing-season droughts are expected to be more severe, requiring significantly more irrigation water to sustain viticulture, even in the most productive zones of the Aude basin.

Chapter 4

Discussion and Conclusion

This thesis set out to develop and apply an advanced agronomic modeling framework to assess the impacts of climate change on agricultural water requirements and crop yields in the Aude basin, a representative Mediterranean watershed. As a contribution to the European-funded PRIMA project, TALANOA-WATER, the primary objective was to provide robust, quantitative inputs for a broader integrated hydro-agro-economic model. This final chapter summarizes the key findings in relation to the initial research questions, discusses their implications for regional water management, acknowledges the study's limitations, and proposes directions for future research.

4.1 Summary of Key Findings

The research presented successfully answered the three core research questions posed in the introduction.

1. Future of Agricultural Water Requirements: The analysis projects a significant increase in irrigation demand for all representative crops throughout the 21st century, with the magnitude of the increase being highly dependent on the emissions pathway. Under the high-emissions RCP 8.5 scenario, the area-weighted mean Net Application (NA) is projected to increase by approximately 40% for PGI Wine and 36% for Tomato by 2100 relative to current levels. This trend is driven by rising temperatures and higher reference evapotranspiration (ET_0). Furthermore, the analysis of extreme years shows that future droughts will be more intense, requiring 15-20% more irrigation water than historical droughts to achieve the same agricultural outcomes.

2. Impact of Water Stress on Crop Yields: The study successfully quantified the relationship between water availability and crop yield by developing production functions for key crops. A critical finding is that for the near-future (2030-2060), soil type is a more dominant factor in determining yield resilience than the differences between climate scenarios. Deep soils with high water holding capacity provide a significant buffer against water stress, maintaining near-maximum yields over a much wider range of water inputs compared to shallow soils. The analysis of a rainfed "safety crop" (Peas) showed that while such adaptation strategies have potential, their viability is severely threatened under high-emissions scenarios.

3. Utility of Integrated Modeling for Policy Support: The modeling framework proved effective at simulating complex, real-world management strategies. The application of the 'SWDPc' factor successfully replicated regulated deficit irrigation for PGI and PDO wines, demonstrating the model's utility for evaluating specific policy rules. Moreover, the comparison of model results with empirical data revealed that current farming practices in the Aude basin already reflect a form of pragmatic deficit irrigation, where farmers accept yields of 80-90% to conserve water. This insight is crucial for designing policies that are aligned with rational farmer behavior.

4.2 Implications and Contribution to Integrated Modeling

The findings of this thesis carry significant implications for the future of agriculture in the Aude basin and other Mediterranean regions. The projected increase in both average and extreme water demand, particularly under high-emission scenarios, suggests that current water management practices may become unsustainable. The strong influence of soil type on crop resilience highlights that adaptation strategies must focus not only on water supply and irrigation technology but also critically on land management practices that enhance soil health and water holding capacity.

This work makes a direct and vital contribution to the integrated modeling objectives of the TALANOA-WATER project.

- **For the Economic Model:** The derived logistic production functions provide a set of simplified, computationally efficient relationships between water input and yield output. These functions serve as a key input to the hydro-agro-economic model, allowing for the rapid assessment of the economic viability and trade-offs of different water allocation policies under a multitude of future scenarios.

- **For the Hydrological Model:** The detailed daily and seasonal outputs of Net Application (NA) and Applied Water (WA) for each crop in every pedoclimatic zone provide spatially explicit water demand data. This information can be integrated into basin-scale hydrological models to better estimate the total demand on surface and groundwater resources, helping to analyze and manage the growing competition for water between agriculture, cities, and ecosystems.

4.3 Limitations and Future Work

While this study provides a comprehensive analysis, it is important to acknowledge its limitations, which also open avenues for future research. The crop area data, while the best available, was not a complete census due to privacy regulations concerning small farms. Future work could benefit from more detailed land use surveys. The main analysis relied on the standard FAO-56 Penman-Monteith equation; incorporating the physiological effects of elevated CO_2 on crop transpiration more deeply remains a key area for further research. Finally, the model assumes static farmer behavior.

Future research should focus on developing a more dynamic framework that allows for farmer adaptation, such as changes in crop choice, irrigation technology, or planting dates in response to changing economic and climatic signals. Expanding the analysis to include a wider range of adaptation strategies would further enhance the model's utility as a policy support tool.

4.4 Conclusion

In conclusion, this thesis successfully developed, validated, and applied a robust agronomic modeling framework that provides critical, quantitative insights into the future of agriculture and water management in the Aude basin. The findings reveal a future of increasing water stress but also highlight the primary importance of soil resilience and the potential for targeted management strategies. By delivering essential data for integrated economic and hydrological modeling, this work provides a valuable tool to support the transition towards a more sustainable and climate-resilient agricultural future.

Bibliography

[1] MedECC et al. *Climate and Environmental Change in the Mediterranean Basin – Current Situation and Risks for the Future. First Mediterranean Assessment Report*. en. Tech. rep. ISBN: 9782957741618 Version Number: 1. MedECC Reports. MedECC Secretariat, Marseille, France., Nov. 2020. DOI: 10.5281/ZENODO.7224821. URL: https://zenodo.org/doi/10.5281/zenodo.7224821 (visited on 03/26/2025).

[2] G. Zittis et al. "Climate Change and Weather Extremes in the Eastern Mediterranean and Middle East". en. In: *Reviews of Geophysics* 60.3 (Sept. 2022), e2021RG000762. ISSN: 8755-1209, 1944-9208. DOI: 10.1029/2021RG000762. URL: https://agupubs.onlinelibrary.wiley.com/doi/10.1029/2021RG000762 (visited on 06/04/2025).

[3] Marta Antonelli and Daniele Fattibene. "The Water-Food Nexus in Mediterranean Cities: The Quest for More Sustainable Diets". en. In: ().

[4] Mohamed Naziq S. et al. "Coupled weather and crop simulation modeling for smart irrigation planning: a review". en. In: *Water Supply* 24.8 (Aug. 2024), pp. 2844–2865. ISSN: 1606-9749, 1607-0798. DOI: 10.2166/ws.2024.170. URL: https://iwaponline.com/ws/article/24/8/2844/103637/Coupled-weather-and-crop-simulation-modeling-for (visited on 06/04/2025).

[5] Noemi Mancosu et al. "SIMETAW# - a Model for Agricultural Water Demand Planning". en. In: *Water Resources Management* 30.2 (Jan. 2016), pp. 541–557. ISSN: 0920-4741, 1573-1650. DOI: 10.1007/s11269-015-1176-7. URL: http://link.springer.com/10.1007/s11269-015-1176-7 (visited on 01/31/2024).

[6] SUWANU EUROPE. "State of play analyses for Occitanie-France". In: ().

[7] SMARR. "PGRE Aude". In: (Mar. 2017).

[8] UMRinnovation INRAe. *Accueil TALANOA-WATER France*. fr. URL: https://talanoa-water-france.hub.inrae.fr/ (visited on 05/14/2025).

[9] *DRIAS, Les futurs du climat - Accueil*. URL: https://www.drias-climat.fr/ (visited on 05/15/2025).

[10] *USGS EROS Archive - Digital Elevation - Global 30 Arc-Second Elevation (GTOPO30) | U.S. Geological Survey*. en. July 2018. URL: https://www.usgs.gov/centers/eros/science/usgs-eros-archive-digital-elevation-global-30-arc-second-elevation-gtopo30 (visited on 05/15/2025).

[11] *GitHub - SantanderMetGroup/convertR: A climate4R package for unit conversion and variable derivation*. URL: https://github.com/SantanderMetGroup/convertR (visited on 05/15/2025).

[12] *Gis Sol » La profondeur des sols en France métropolitaine*. en. URL: https://www.gissol.fr/donnees/cartes/la-profondeur-des-sols-en-france-metropolitaine-1493 (visited on 05/18/2025).

[13] *Gis Sol » Les réserves en eau utile de la France métropolitaine*. URL: https://www.gissol.fr/donnees/cartes/les-reserves-en-eau-utile-de-la-france-metropolitaine-1483 (visited on 05/18/2025).

[14] FAO. *FAO documentation for ET*. URL: https://www.fao.org/3/X0490E/X0490E00.htm.

[15] *RCP Database*. URL: https://tntcat.iiasa.ac.at/RcpDb/dsd?Action=htmlpage&page=download (visited on 05/19/2025).

[16] Andrew D. B. Leakey et al. "Elevated CO2 effects on plant carbon, nitrogen, and water relations: six important lessons from FACE". en. In: *Journal of Experimental Botany* 60.10 (July 2009), pp. 2859–2876. ISSN: 1460-2431, 0022-0957. DOI: 10.1093/jxb/erp096. URL: https://academic.oup.com/jxb/article-lookup/doi/10.1093/jxb/erp096 (visited on 05/19/2025).

[17] *Les restrictions sécheresses se durcissent 28/08/2023 – SMMAR*. fr-FR. URL: https://www.smmar.fr/restrictions-secheresse-280823/ (visited on 06/10/2025).

[18] Sam Geerts and Dirk Raes. "Deficit irrigation as an on-farm strategy to maximize crop water productivity in dry areas". en. In: *Agricultural Water Management* 96.9 (Sept. 2009), pp. 1275–1284. ISSN: 03783774. DOI: 10.1016/j.agwat.2009.04.009. URL: https://linkinghub.elsevier.com/retrieve/pii/S0378377409001243 (visited on 06/10/2025).

[19] Kassam Doorenbos. *FAO Irrigation and Drainage Paper 33*. 1979.

[20] J C van Dam et al. "Theory of SWAP version 2.0". en. In: ().

[21] Sotirios V. Archontoulis and Fernando E. Miguez. "Nonlinear Regression Models and Applications in Agricultural Research". en. In: *Agronomy Journal* 107.2 (Mar. 2015), pp. 786–798. ISSN: 0002-1962, 1435-0645. DOI: 10.2134/agronj2012.0506. URL: https://acsess.onlinelibrary.wiley.com/doi/10.2134/agronj2012.0506 (visited on 06/28/2025).

APPENDIX

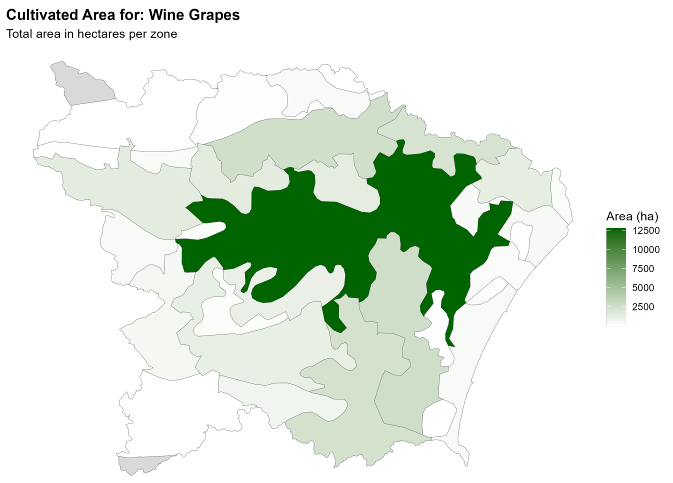

(a) Wine Grapes

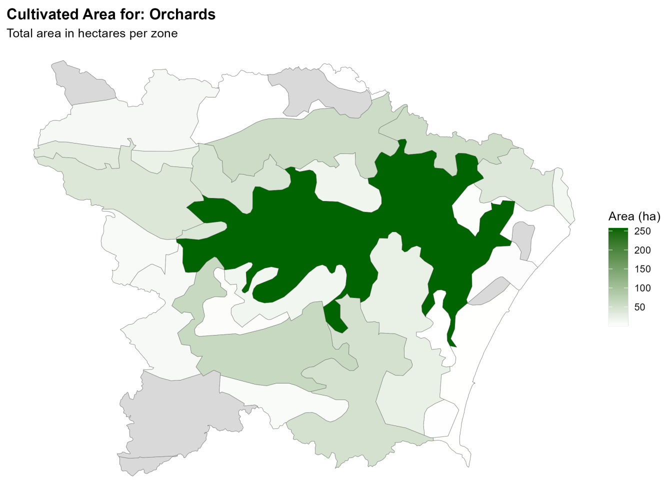

(b) Orchards

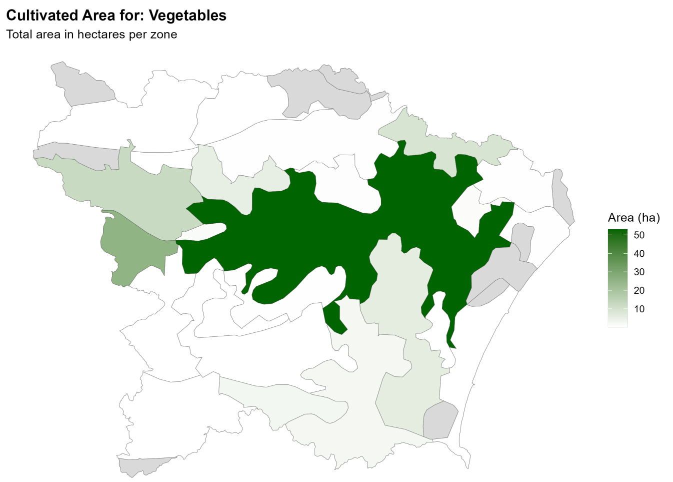

(c) Vegetables

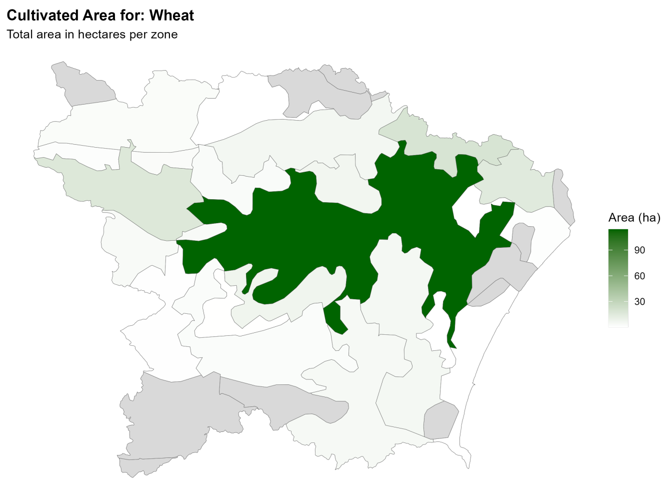

(d) Wheat

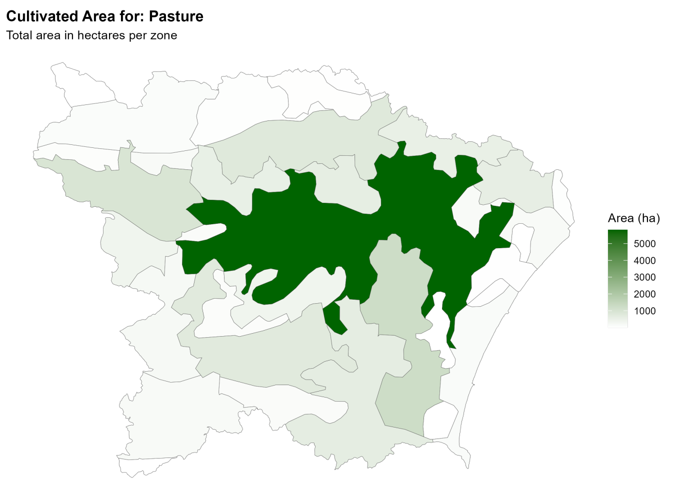

(e) Pasture

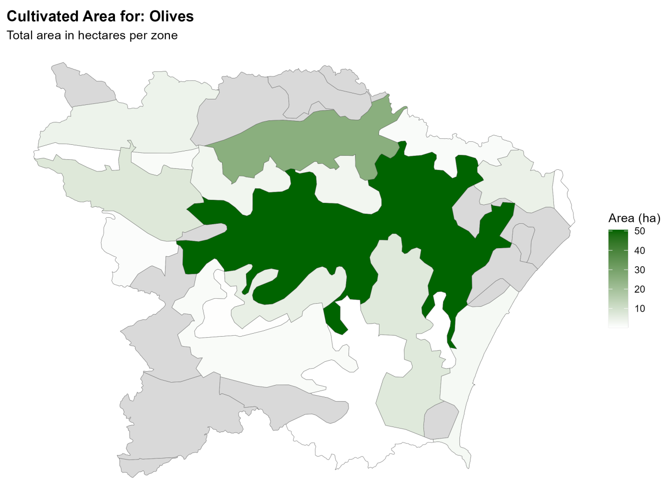

(f) Olives

Figure 1: Spatial distribution of major crop groups in the Aude Basin. Each map shows the total cultivated area (in hectares) per zone for that group. The color scale on each map is independent.